

Grant Agreement No 727689



**Document Title:**

Effect of sea water aging on the static and fatigue properties of composites for tidal blade design

**REALTIDE Document No:**

RLT-WP1-T3-TNO-000-00

Status Code	Description
A	Accepted
B	Issued for Acceptance
C	Issued for Review
D	Information Only Approval Not Required
E	Cancelled

					
00	D	-	Mael Arhant 07/12/19	Peter Davies 10/12/19	
Rev No	Status	Revision Description	Prepared By / Date	Reviewed By / Date	Approved By / Date

**IFREMER reference: RDT/LCSM 19-249**



## Table of Contents

<b>1.</b>	<b>INTRODUCTION .....</b>	<b>2</b>
<b>2.</b>	<b>MATERIALS &amp; METHODS.....</b>	<b>3</b>
<b>2.1</b>	<b>Materials .....</b>	<b>3</b>
<b>2.2</b>	<b>Physico-chemical characterization.....</b>	<b>4</b>
2.2.1	Differential Scanning Calorimetry .....	4
2.2.2	Fibre Volume Content .....	4
2.2.3	Void Content.....	4
<b>2.3</b>	<b>Mechanical tests .....</b>	<b>5</b>
2.3.1	Static tests .....	5
2.3.2	Fatigue tests .....	7
<b>3.</b>	<b>QUALITY CONTROL .....</b>	<b>8</b>
<b>3.1</b>	<b>Curing Conditions.....</b>	<b>8</b>
<b>3.2</b>	<b>Fibre volume content.....</b>	<b>9</b>
<b>3.3</b>	<b>Void Content .....</b>	<b>10</b>
3.3.1	Ultrasonic C-Scan .....	10
3.3.2	Optical microscopy.....	12
<b>4.</b>	<b>SEA WATER AGING – KINETICS .....</b>	<b>14</b>
<b>4.1</b>	<b>Kinetics of water absorption within the resin .....</b>	<b>15</b>
4.1.1	Effect of temperature on water absorption .....	15
4.1.2	Effect of sample thickness on water absorption .....	15
4.1.3	Desorption at 60°C .....	16
4.1.4	Water diffusion modelling within the resin .....	17
4.1.5	Conclusion.....	18
<b>4.2</b>	<b>Kinetics of water absorption within the composites.....</b>	<b>18</b>
4.2.1	Effect of temperature on water absorption .....	18
4.2.2	Effect of stacking sequence on water absorption .....	22
4.2.3	Desorption at 60°C .....	23
<b>4.3</b>	<b>Conclusion .....</b>	<b>24</b>
<b>5.</b>	<b>MECHANICAL TESTS - STATIC PROPERTIES.....</b>	<b>24</b>
<b>5.1</b>	<b>Static properties in the unaged state .....</b>	<b>26</b>
5.1.1	Tensile tests.....	26



5.1.2	Interlaminar Shear Strength tests (ILSS).....	31
5.1.3	Flexural properties .....	31
<b>5.2</b>	<b>Static properties in sea water in the saturated state.....</b>	<b>33</b>
5.2.1	Tensile tests.....	33
5.2.2	Flexural properties .....	37
5.2.3	Conclusion .....	39
<b>5.3</b>	<b>Static properties after water desorption .....</b>	<b>39</b>
<b>6.</b>	<b>MECHANICAL TESTS – FATIGUE PROPERTIES .....</b>	<b>42</b>
<b>6.1</b>	<b>Fatigue properties in the unaged state .....</b>	<b>42</b>
6.1.1	Comparison between carbon/epoxy laminates with different stacking sequences .....	42
6.1.2	Comparison between carbon/epoxy and glass/epoxy laminates with the same stacking sequence.....	43
<b>6.2</b>	<b>Fatigue properties in the aged state.....</b>	<b>43</b>
<b>6.3</b>	<b>Fatigue properties after water desorption.....</b>	<b>45</b>
<b>7.</b>	<b>CONCLUSION.....</b>	<b>46</b>

## 1. INTRODUCTION

The RealTide project aims to identify main failure causes of tidal turbines at sea and to provide a step change in the design of key components, namely the blades and power take-off systems, adapting them more accurately to the complex environmental tidal conditions. Composite blades are a critical element in these turbines, so their long term behaviour must be fully understood if turbine reliability is to be ensured. Two of the potential failure modes are degradation due to prolonged seawater exposure and damage initiation and propagation by cyclic (fatigue) loading. For this reason, a test campaign was initiated to study these two aspects.

Most tidal turbine prototypes have been manufactured from carbon fibre reinforced composites, but these materials are expensive. It has been suggested that replacing carbon fibres by glass might result in significant cost savings. However, such a decision must be based on a complete set of material property data, both before and after seawater aging, so this was included in the test programme. Quasi-static test data have also been generated, as they are essential for designing these blades.

This document contains results from this sea water aging test campaign, which was performed within WP 1.3 of the RealTide project. Figure 1 shows a schematic diagram indicating where these tests are located within the RealTide project.

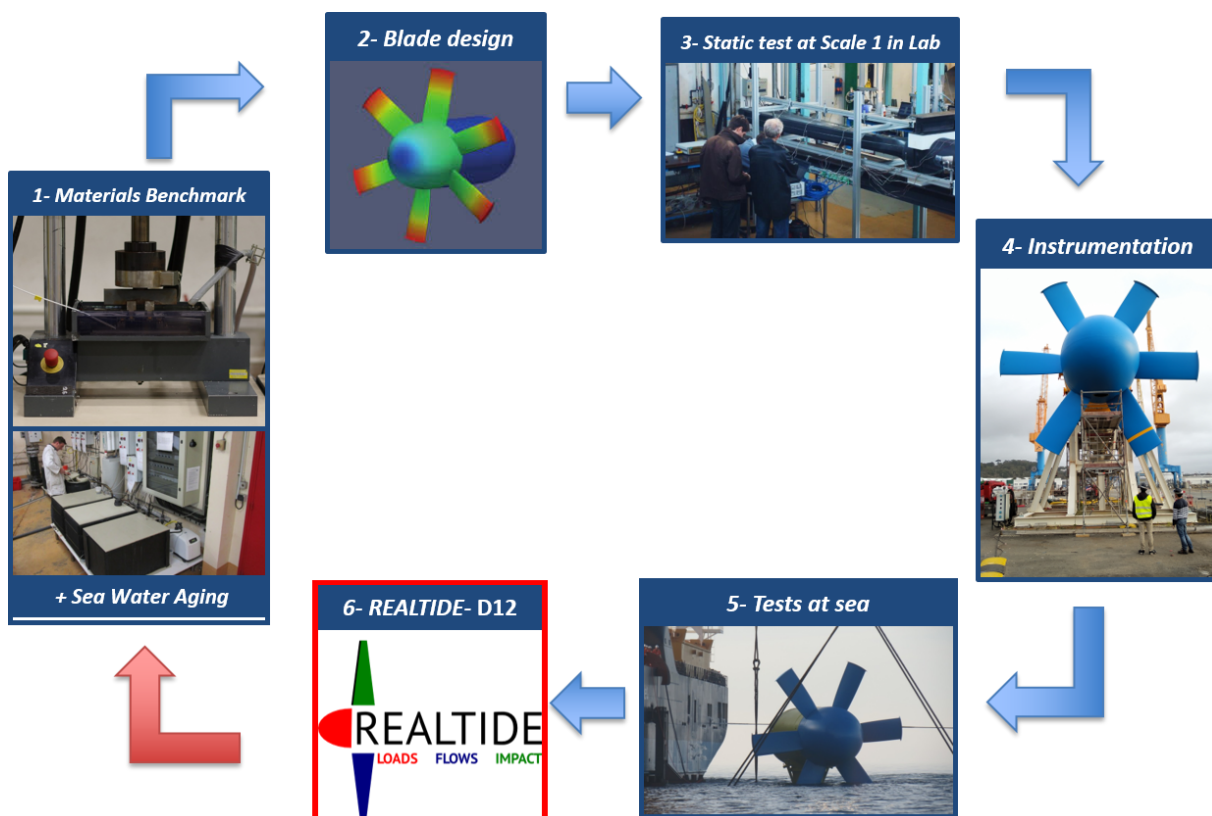


Figure 1: Flowchart

In a previous study at IFREMER of the carbon/epoxy composites employed by Sabella for the D10 blades some seawater aging tests were performed. These provided initial data to validate the material choice for the prototype and to suggest that the material was not very sensitive to seawater immersion, Figure 2. However, cyclic tests after aging were not performed at the time.

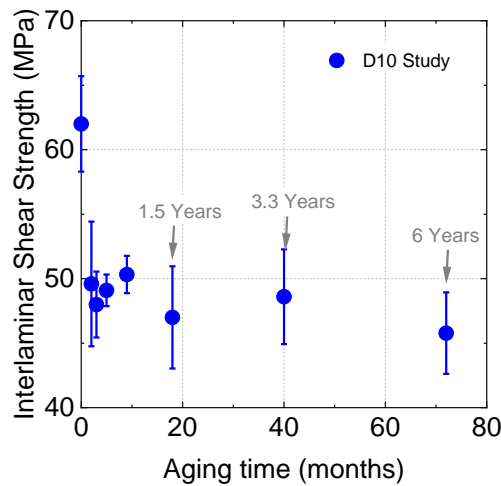


Figure 2: Effect of sea water aging at 60°C on the Interlaminar shear strength

## 2. MATERIALS & METHODS

### 2.1 Materials

Eight panels were produced by a high performance composite manufacturer, Multiplast (Vannes, France) using resin infusion. The resin was supplied by Sicomin and is a high performance resin for infusion (Resin: SR1710; Hardener: SD 8823), with a fully cured T<sub>g</sub> slightly above 100°C. All the panels studied here were cured at 60°C for 12 hours. Table 1 shows the nine materials studied, which include unreinforced resin and 4 lay-ups of that resin reinforced with each of carbon and glass fibres. The unidirectional and ±45 materials were used to obtain basic design data, before and after seawater aging, the 0/90 and 0/45° laminates were used for cyclic tests and are more representative of the blade stacking sequences.

Table 1: Materials, sequences and fibre weight used for the project

Material		Reference	Sequence	Fibre Weight (g/m <sup>2</sup> )	Thickness (mm)
Neat Resin	SR1710-SD8823	R1	/	/	2.5
Carbon/Epoxy	T700/SR1710-SD8823	P1	[0] <sub>2s</sub>	600	2.1 ± 0.1
Carbon/Epoxy	T700/SR1710-SD8823	P2	[±45] <sub>2s</sub>	600	2.4 ± 0.1
Carbon/Epoxy	T700/SR1710-SD8823	P3	[0/±45] <sub>s</sub>	600	2.4 ± 0.1
Carbon/Epoxy	T700/SR1710-SD8823	P4	[0/90] <sub>s</sub>	600	2.1 ± 0.1
Glass/Epoxy	L600/SR1710-SD8823	P5	[0] <sub>2s</sub>	600	3.7 ± 0.1
Glass/Epoxy	L600/SR1710-SD8823	P6	[±45] <sub>2s</sub>	600	2.7 ± 0.1

Glass/Epoxy	L600/SR1710-SD8823	P7	[0/±45] <sub>s</sub>	600	3.2 ± 0.1
Glass/Epoxy	L600/SR1710-SD8823	P8	[0/90] <sub>s</sub>	600	3.6 ± 0.1

## 2.2 Physico-chemical characterization

### 2.2.1 Differential Scanning Calorimetry

The curing conditions were checked using DSC on Q200 equipment from TA Instruments™. Samples extracted from the panels were used.

First, the given sample was heated from 0°C up to 200°C at a heating ramp of 10°C/min. Then, this same sample was cooled down to ambient temperature and a second heating stage was carried out again at 10°C/min up to 200°C. These two heating stages allow us to determine if there is an evolution in the T<sub>g</sub>.

### 2.2.2 Fibre Volume Content

Fibre volume content was determined from matrix burn off tests coupled with density measurements using the following equation:

$$V_f = \frac{W_f \rho_c}{\rho_f}$$

Where W<sub>f</sub> is the fibre weight fraction and ρ<sub>c</sub> and ρ<sub>f</sub> are respectively the densities of the composite and the fibres. It was first checked by TGA (thermogravimetric analysis under inert gas) that this burn-off procedure did not result in weight change due to oxidation of carbon fibres. Fibre densities for the glass and carbon fibres were respectively taken as 2.54 g.cm<sup>3</sup> and 1.76 g.cm<sup>3</sup>.

The fibre weight content W<sub>f</sub> was determined from matrix burn off tests performed at 450°C for 2 hours. For each condition, three specimens with dimensions equal to 30 x 30 x thickness mm<sup>3</sup> were used, Figure 3. Densities of each material were measured using a gas pycnometer.

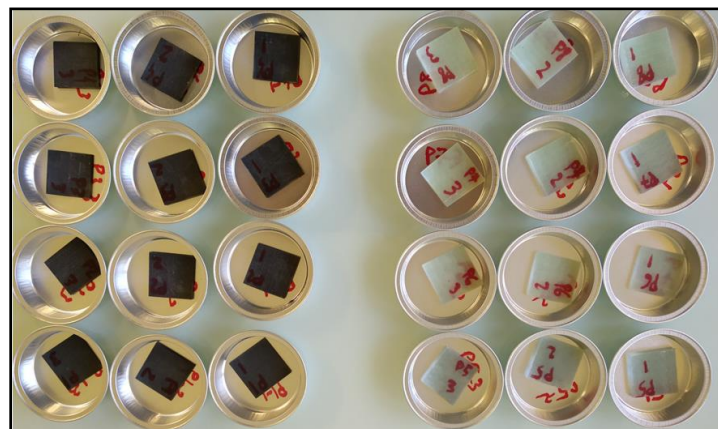


Figure 3: Specimens for burn off tests

### 2.2.3 Void Content

#### 2.2.3.1 Ultrasonic C-Scan



In order to check the overall quality of a given composite panel, ultrasound scanning is very useful because the classic imaging techniques only concern very small specimens. With ultrasonic C-scan, the through thickness attenuation contained inside a given composite panel can be investigated. However, the results obtained are only qualitative and not quantitative. A Sofratest™ ultrasonic inspection system was used to measure through thickness attenuation using 5 MHz focused transducers by placing the given composite panel in a water tank.

### 2.2.3.2 Optical microscopy

The quality in terms of voids of the different panels that were manufactured was checked using optical microscopy with a LEICA™ DM ILM microscope, on sections polished using several sandpaper grades (320, 600, 1200, 2400 and 4000).

## 2.3 Mechanical tests

### 2.3.1 Static tests

Results will be presented from two types of mechanical test: in-plane tension and out-of-plane bending and short beam shear.

#### 2.3.1.1 Tensile tests

Tensile tests were performed according to ISO 527 on an Instron testing machine using a load cell of 200 kN at a crosshead speed of 2 mm/min. These were carried out on  $[0^\circ]$ ,  $[90^\circ]$  and  $[\pm 45^\circ]$  specimens, i.e. on specimens taken from panels 1, 2, 5 and 6 (Table 1). All the specimens were tabbed using glass/epoxy tabs with a sequence of  $[\pm 45]$ . For each condition, five specimens were tested. Strain was measured using two different methods, Figure 4:

- A mechanical extensometer with a gauge length of 50 mm to measure strain in the longitudinal direction
- Digital Image Correlation (DIC) to measure the longitudinal and transverse strains

These tests provide values of  $E_1$ ,  $E_2$ ,  $\nu_{12}$  and  $G_{12}$ , together with  $\sigma_1$ ,  $\sigma_2$  and  $\tau_{12}$ . Modulus values were calculated as the slopes of the stress-strain plots over the strain range 0.1-0.3%. Stress for the tests on unidirectional materials was taken as  $\sigma = \frac{L}{S}$ . For the tests on specimens at  $[\pm 45^\circ]$  stress was taken as  $\tau_{12} = \frac{\sigma_{12}}{2.S}$ . Shear strain was taken as  $\gamma_{12} = \varepsilon_y - \varepsilon_x$

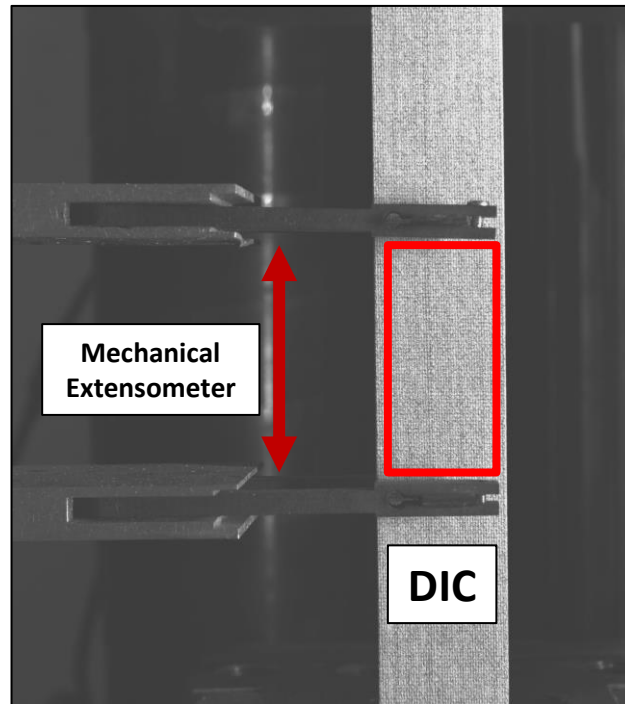


Figure 4: Mechanical extensometer and DIC used for tensile tests

### 2.3.1.2 Four point bending tests

Four point bending tests were performed at a crosshead speed of 1mm/min. The dimensions of the carbon/epoxy specimens are 140 x 25 x 2 mm<sup>3</sup> and those of the glass/epoxy are 120 x 25 x 3 mm<sup>3</sup>.

### 2.3.1.3 Interlaminar Shear Strength tests (ILSS)

Interlaminar shear strength tests were performed on unidirectional 0° specimens (Panels P1 and P5), according to ISO 14 130 (support length/thickness = 5) on an Instron™ testing machine using a 10 kN load cell, Figure 5. These were performed at a crosshead speed of 1 mm/min until delamination occurred. For each condition, five specimens were tested to failure. The apparent Interlaminar Shear Strength  $\tau_{13}$  was measured using the following equation :

$$\tau = \frac{3}{4} \times \frac{F}{bh}$$

Where F is the load in N. b and h are respectively the width and the thickness of the tested specimen.



Figure 5: ILSS test fixture

### 2.3.2 Fatigue tests

Fatigue tests on carbon/epoxy specimens were performed on a 25 kN Zwick hydraulic test frame for four point flexure using  $(140 \times 25 \text{ mm}^2)$  rectangular specimens with 60 mm between upper loading points and 120 mm between lower supports, Figure 6. Tests were performed at a frequency of 2 Hz using an R-ratio of 0.1. All flexural tests were performed immersed in continuously renewed seawater at 25°C.

First tests on the glass/epoxy specimens were performed in the same way. However, due to the lower stiffness of these specimens, the deflection seen during the tests was too large for the test frame. Therefore, dimensions were adjusted by reducing the span (specimens :  $120 \times 25 \text{ mm}^2$ , 50 mm between upper loading points and 100 mm between lower supports).



Figure 6: Fatigue four point bending testing machine

### 3. QUALITY CONTROL

#### 3.1 Curing Conditions

The initial curing conditions were checked by DSC. An example of a DSC thermogram is shown in Figure 7 for an unidirectional carbon/epoxy specimen. It may be noted that this type of thermogram was recorded for all the composite panels considered in this study.

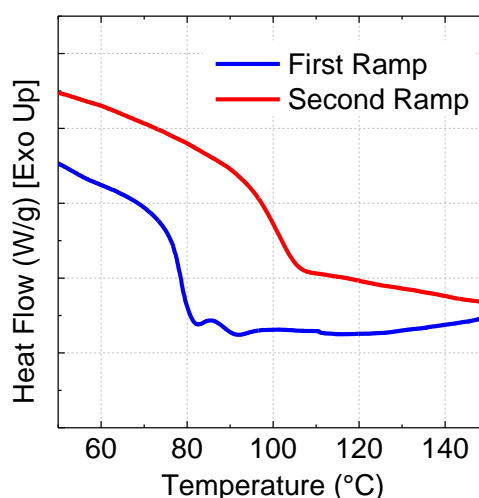


Figure 7: Cure conditions in the unaged state

Analysis of plots such as the one shown in Figure 7 reveals that the glass transition temperature increases after the second heating ramp, suggesting that the resin was not fully cured in its initial state. The  $T_g$  after the second ramp was about 102°C for all the specimens considered in this study, which corresponds to the value given by Sicomin (the resin supplier) for a fully cured resin.

The glass transition temperature values for all the materials (one sample per panel) corresponding to the first heating ramp are shown in Table 2.

**Table 2: Results from DSC tests performed on the different composite panels**

Material	Composite	Sequence	T <sub>g</sub> (°C)
Neat resin	/	/	95
Carbon/Epoxy	P1	[0]	79
	P2	[±45]	75
	P3	[0/±45]	77
	P4	[0/90]	87
Glass/Epoxy	P5	[0]	87
	P6	[±45]	75
	P7	[0/±45]	76
	P8	[0/90]	78

### 3.2 Fibre volume content

The results from fibre volume content measurements as well as density measurements are shown in Table 3.

**Table 3: Fibre volume content and densities measured on the different composite panels**

Material	Composite	Sequence	V <sub>f</sub> (%)	ρ <sub>c</sub> (g/cm <sup>3</sup> )
C/Epoxy	P1	[0]	58.4 ± 0.2	1.46 ± 0.01
	P2	[±45]	46.5 ± 1.8	1.33 ± 0.05
	P3	[0/±45]	53.4 ± 0.4	1.41 ± 0.01
	P4	[0/90]	58.4 ± 0.8	1.47 ± 0.03
G/Epoxy	P5	[0]	50.9 ± 0.4	1.81 ± 0.01
	P6	[±45]	52.2 ± 0.2	1.83 ± 0.01

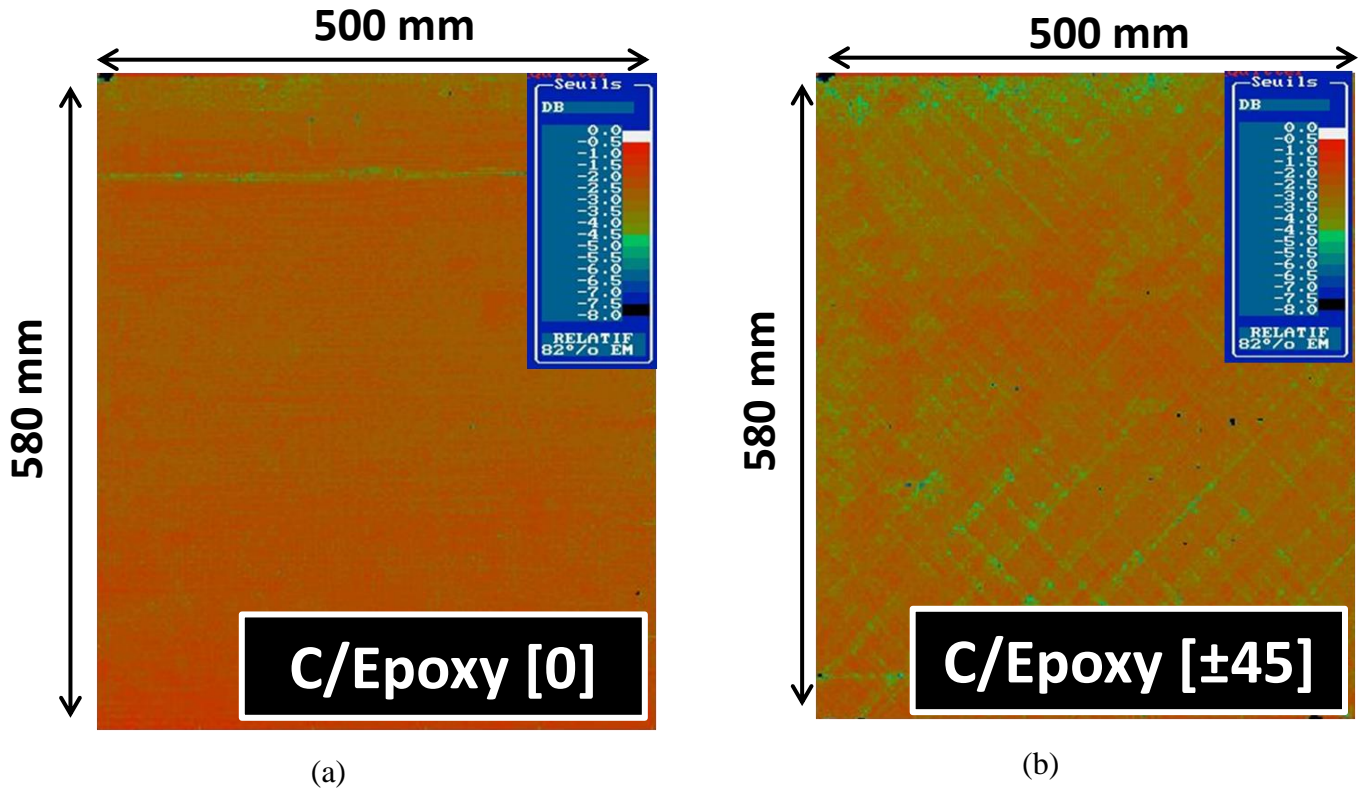
	P7	[0/±45]	50.8 ± 1.0	1.80 ± 0.02
	P8	[0/90]	50.0 ± 0.6	1.80 ± 0.01

The values for the glass fibre reinforced panels are quite similar, in the range 50-52%, but the carbon composite results are more variable with a significantly lower value for the composites containing ±45° reinforcement.

### 3.3 Void Content

#### 3.3.1 Ultrasonic C-Scan

Ultrasonic C-scan results for the carbon/epoxy and glass/epoxy panels are respectively shown in Figures 8 and 9. Based on experience, high levels of through thickness attenuation (over 20dB) usually correspond to the presence of macrovoids, i.e. significant defects. On the other hand, low levels of attenuation (below 10 dB) indicate good panel quality (small amounts of microvoids or none).



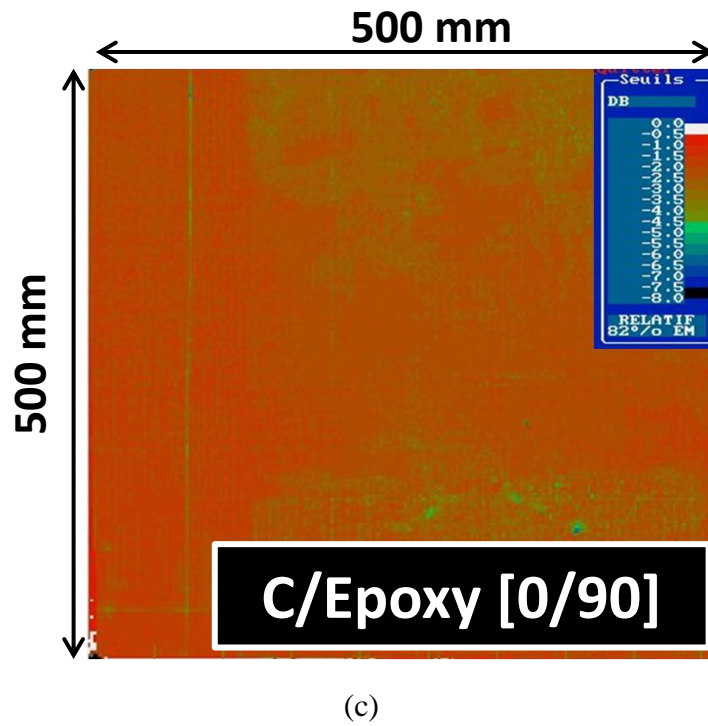
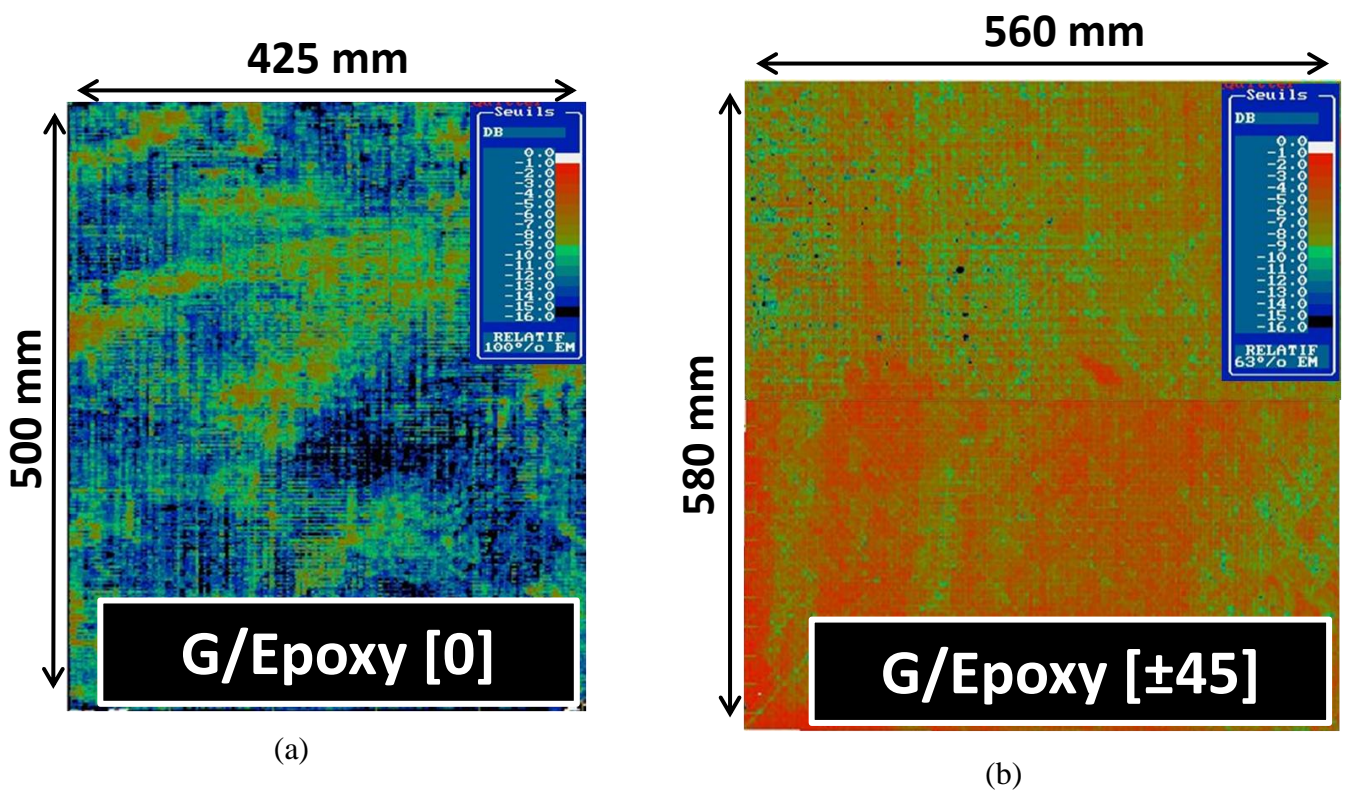
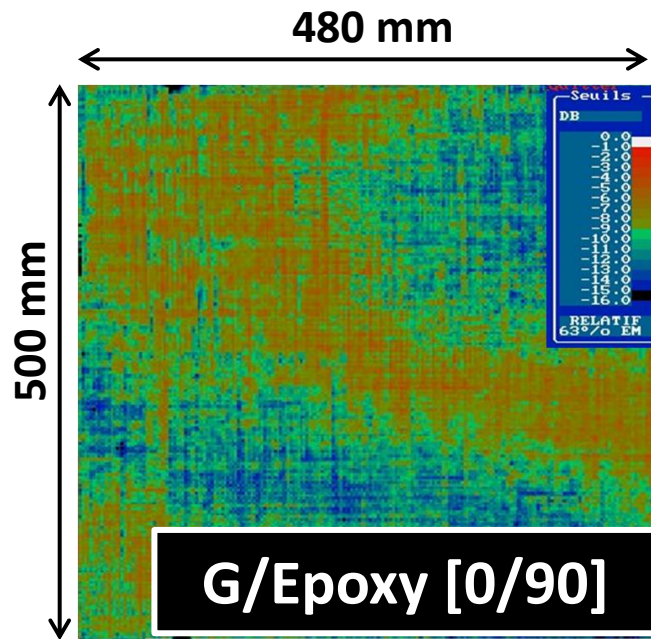


Figure 8: C-scans for the carbon/epoxy panels - Scale : 0 to 8dB (a) [0] (b) [±45] (c) [0/90]

Results from ultrasonic C-scans on carbon/epoxy composites indicate that these panels are of excellent quality in terms of voids, with attenuation levels mostly lower than 6 dB. These results were confirmed by optical microscopy (see following section).





(c)

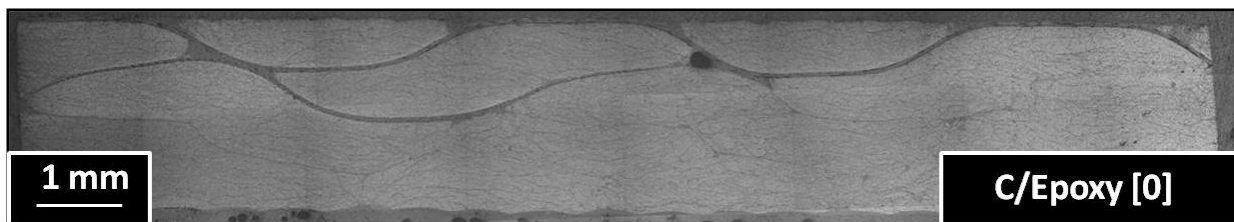
Figure 9: C-scans for the glass/epoxy panels - Scale: 0 to 16dB (a) [0] (b) [ $\pm 45$ ] (c) [0/90]

Results from ultrasonic C-scans on glass/epoxy composites indicate that these panels are of a different quality compared with the carbon/epoxy panels. Through thickness attenuations are much higher than those observed on the carbon/epoxy panels (note the different scale, 16 dB instead of 8dB for the carbon composites).

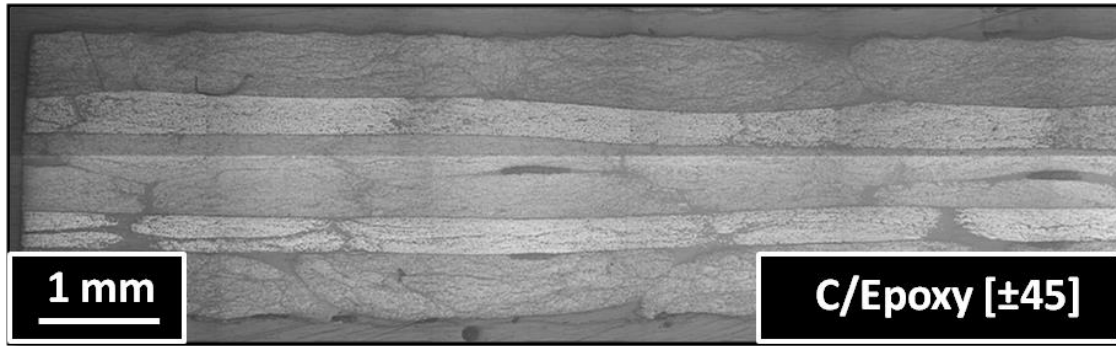
For the unidirectional glass/epoxy panel, observed attenuations are around 10 dB or higher, which might indicate the presence of macrovoids. This will be checked later using optical microscopy. Results are quite similar for the glass/epoxy panel with a [0/90] sequence. However, the glass/epoxy panel with a [ $\pm 45$ ] sequence shows through thickness attenuation around 10 dB or lower, which indicates a panel of a better quality than the other two in terms of voids.

### 3.3.2 Optical microscopy

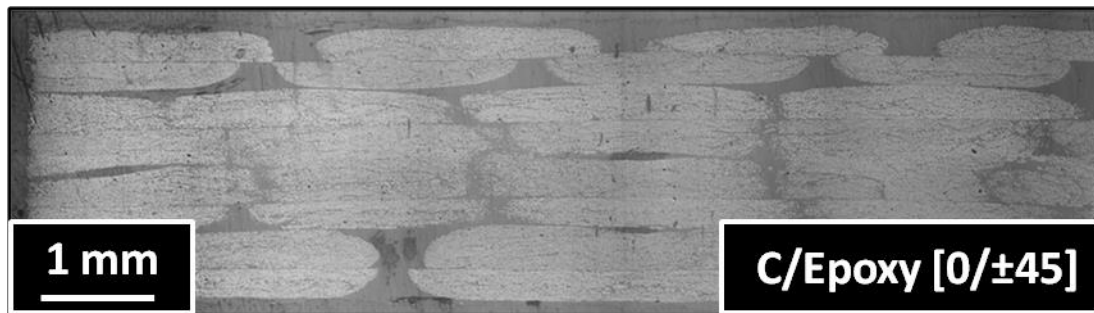
Results from polished sections for carbon/epoxy and glass/epoxy panels are now respectively shown in Figures 10 and 11.



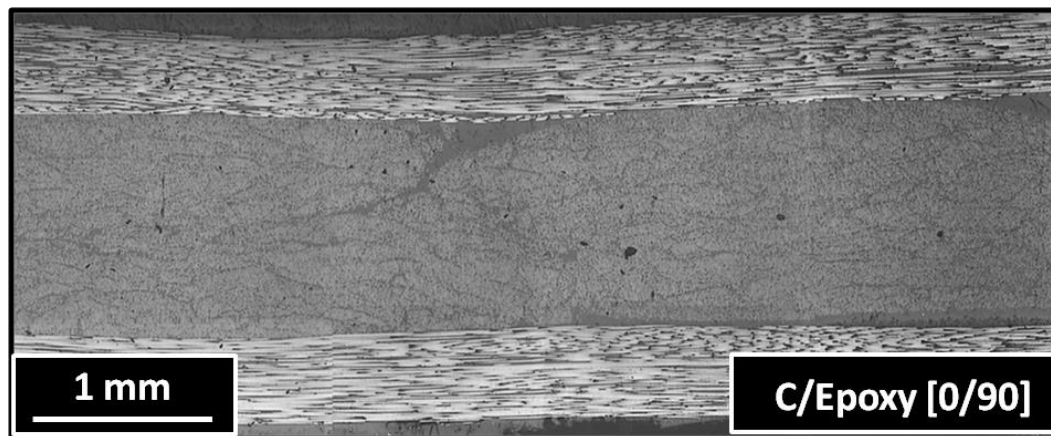
(a)



(b)



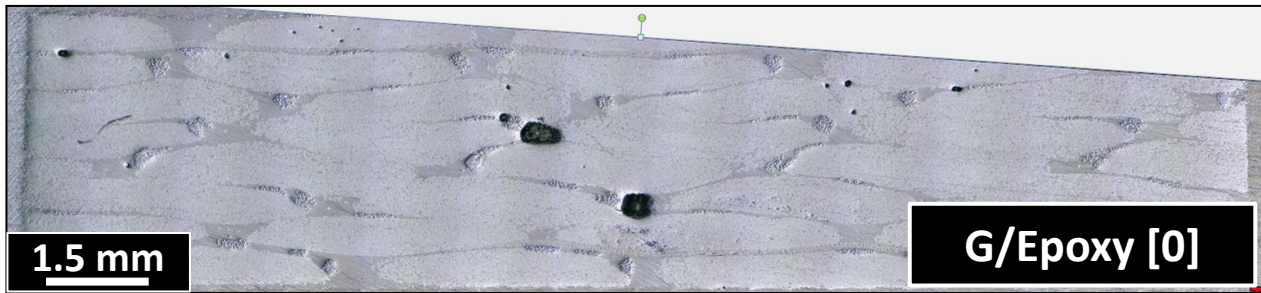
(c)



(d)

Figure 10: Polished sections for specimens extracted from the carbon/epoxy panels (a) [0] (b) [±45] (c) [0/±45] (d) [0/90]

The images in Figure 10 show that the carbon/epoxy panels used in this study are of excellent quality in terms of voids, which is in accordance with results from ultrasonic C-scans.



(a)



(b)



(c)



(d)

Figure 11: Polished sections for specimens extracted from the glass/epoxy panels (a) [0] (b) [±45] (c) [0/±45] (d) [0/90]

On the other hand, results in Figure 11 show that the glass/epoxy composite panels contain some macrovoids throughout the thickness, which explains the higher through thickness U/S attenuation observed on Figure 8. It is important to highlight these macrovoids, as they are likely to have a important effect on the fatigue life of such laminates.

#### 4. SEA WATER AGING – KINETICS

The kinetics of water absorption are investigated in this section. These are important, as if models for water ingress can be developed then the water profiles within composite structures can be evaluated, and related to changes in mechanical behaviour with time.

First, results from weight gain measurements performed on the neat resin at different temperatures are presented. Then, weight increases during immersion of the glass and carbon reinforced composites are presented and discussed. The samples presented in this section were all immersed in sea water for a duration of one year at different temperatures.

#### 4.1 Kinetics of water absorption within the resin

This section is devoted to the water absorption in the resin only, without fibres. The aim of this section is to investigate whether or not the water absorption kinetics can be described using a Fickian model. In most polymers, water sorption follows a Fickian behaviour, i.e., the water diffusion can be described as follows using a diffusion coefficient  $D$  and a mass at saturation  $M_{\infty}$ :

$$\frac{M(t)}{M_{\infty}} = 1 - \frac{8}{\pi^2} \sum_i \frac{1}{(2i + 1)^2} \exp\left(-\frac{D(2i + 1)^2 \pi^2 t}{h^2}\right)$$

Where  $h$  is the sample thickness in mm and  $t$  the immersion time in s. The diffusion coefficient can be calculated from the initial linear part of the sorption curve where  $\frac{M(t)}{M_{\infty}} \leq 0.5$  using the following equation:

$$D = \frac{\pi}{16} \cdot \frac{h^2}{t} \left(\frac{M(t)}{M_{\infty}}\right)^2$$

##### 4.1.1 Effect of temperature on water absorption

First, the effect of water temperature on the water absorption is shown in Figure 12.

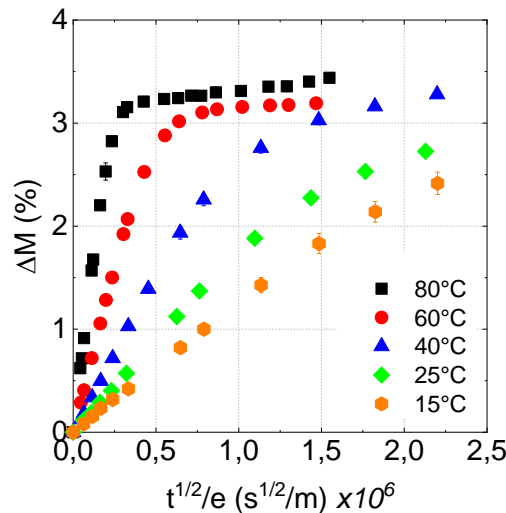


Figure 12: Effect of temperature on the water absorption within the resin

Results show that the lower the temperature the slower the water diffusion. Therefore, this figure confirms that increasing the water temperature accelerates the sea water aging process. Also, water saturation is reached at values close to 3.2 % weight gain.

##### 4.1.2 Effect of sample thickness on water absorption

For modelling purposes, it is necessary to investigate the effect of sample thickness on the water diffusion. Results are shown in Figure 13. These show that the thicker the specimen the slower the water diffusion. Also, water diffusion can be described using a fickian law using a unique water diffusion coefficient and mass at saturation, indicating that this model may be used for thicker structures.

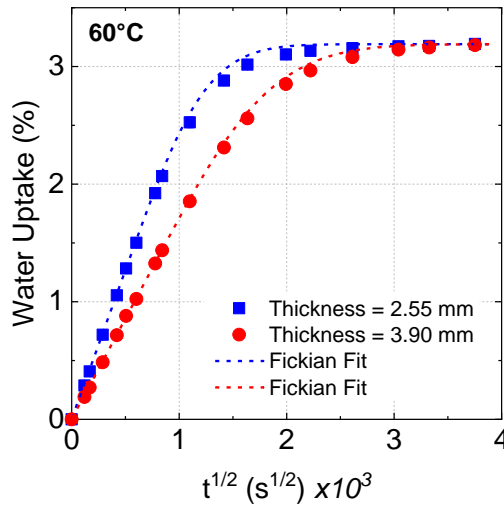


Figure 13: Effect of sample thickness on the water diffusion on the neat resin

#### 4.1.3 Desorption at 60°C

The first mechanism which leads to changes in epoxy resin properties during immersion is usually plasticization. This is a reversible mechanism which promotes reduced modulus and yield stress but increased ductility. In order to investigate the reversibility of plasticization, samples were dried after aging. Results are shown in Figure 14 for immersion and drying at 60°C. These results show that the water sorption process is not fully reversible here, as the water content at the end of the desorption process does not reach the initial unaged mass. This suggests that there may be some surface oxidation at this temperature.

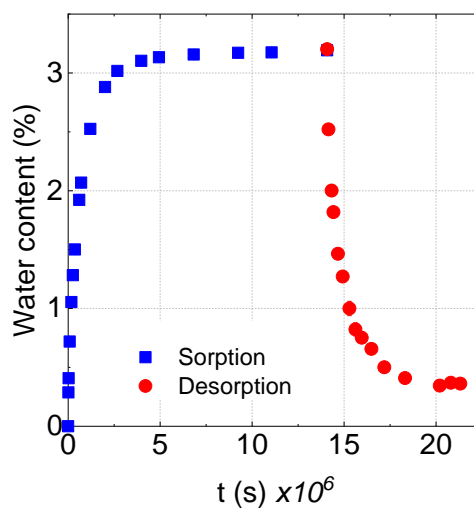


Figure 14: Effect of water sorption and desorption on the water diffusion

#### 4.1.4 Water diffusion modelling within the resin

In order to be able to determine the accelerating effect of immersion at higher temperature it is very useful to know whether an Arrhenius relationship can be applied. Therefore, the effect of water temperature on the water diffusion kinetics was examined. Results for 5 temperatures are presented in Figure 15.

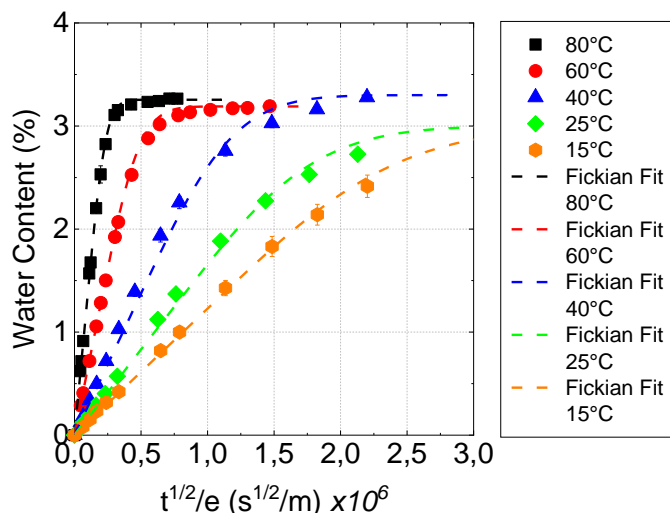


Figure 15: Effect of water temperature on the water diffusion kinetics in the neat resin

First, these results show that water temperature does have a significant effect on the water diffusion. The higher the temperature the faster the diffusion. Then, assuming a Fickian model for each condition investigated, the mass at saturation and associated water diffusion coefficients were determined as shown in Table 4. It may be noted that after one year of aging, only the specimens immersed at 80, 60 and 40°C were fully saturated with water. This means that the masses at saturation for the 25 and 15°C specimens were extrapolated here, not measured.

Table 4: Water diffusion parameters for the neat resin at different temperatures

T (°C)	M <sub>∞</sub> (%)	D (m <sup>2</sup> /s)
80	3.3 ± 0.1	3.48.10 <sup>-12</sup>
60	3.2 ± 0.1	8.08.10 <sup>-13</sup>
40	3.3 ± 0.1	1.45.10 <sup>-13</sup>
25	3.0*	6.03.10 <sup>-14</sup> *
15	3.1*	3.29.10 <sup>-14</sup> *

Results in Table 4 show that for all the water temperatures investigated here, the mass at saturation is similar, around 3.2%. Then, as the temperature increases, the water diffusion coefficient also increases. These diffusion coefficients, plotted in Figure 16, allow us to show that water diffusion can be described to a first approximation using an Arrhenius law using the following equation:

$$D = D_0 \cdot \exp\left(-\frac{E_a}{RT}\right)$$

Where  $D$  is the diffusion coefficient,  $D_0$  the pre exponential diffusion coefficient in  $m^2/s$ ,  $E_a$  the activation energy,  $R$  the gas constant equal to  $8.31 J.mol^{-1}.K^{-1}$  and  $T$  the temperature in  $K$ .

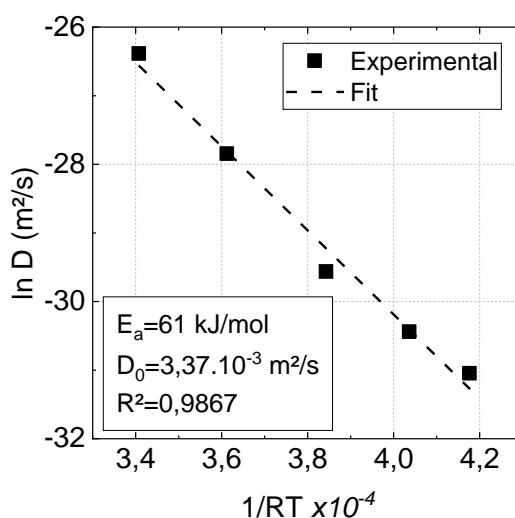


Figure 16: Measured diffusion coefficient  $D$  as a function of  $1/RT$  in the neat resin

#### 4.1.5 Conclusion

This section was devoted to the water absorption within the resin. Results have shown that the water absorption kinetics can be described using a Fickian model. This was confirmed on samples immersed at different temperatures but also on specimens of different thicknesses.

### 4.2 Kinetics of water absorption within the composites

It was shown in the previous section that the water absorption within the unreinforced resin can be modelled. This section is now devoted to the composites, both carbon and glass.

#### 4.2.1 Effect of temperature on water absorption

First, the effect of temperature is investigated for both the carbon/epoxy and glass/epoxy composites in Figures 17a and 17b, respectively. It may be noted that in these two figures only the unidirectional specimens (panels identified as P1 and P5) are represented. It will be shown later that the stacking sequence has very little effect on the water diffusion.

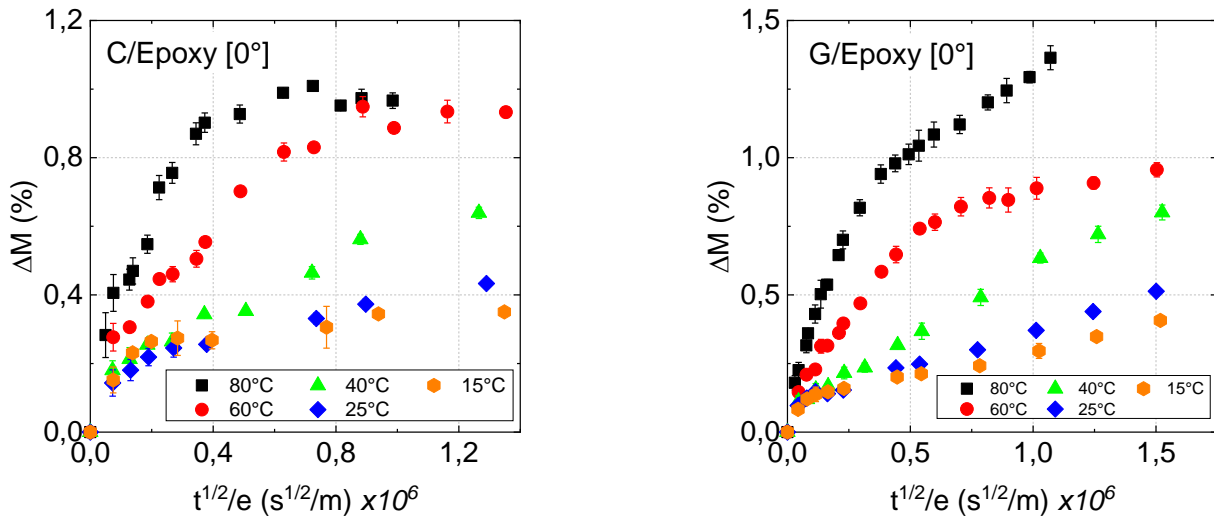


Figure 17 : Effect of temperature on the water absorption kinetics for (a) Carbon/Epoxy (b) Glass/Epoxy composites

The first conclusion that may be drawn is that for both composites, the higher the temperature the faster the water diffusion. This conclusion is similar for all stacking sequences investigated here.

Second, compared with the weight gain data shown in Figure 15 on the neat resin, if we look more closely, plots are quite different. If water diffusion can be described using a simple Fickian law, water diffusion should be linear in the first part of the plot and should saturate towards a certain water value, which is not the case in these plots. For both the carbon and glass laminates, an initial water diffusion process that seems independent of the water temperature is observed. This phenomenon is shown more clearly in Figure 18 by reducing the scale to the very first water absorption points of the plots.

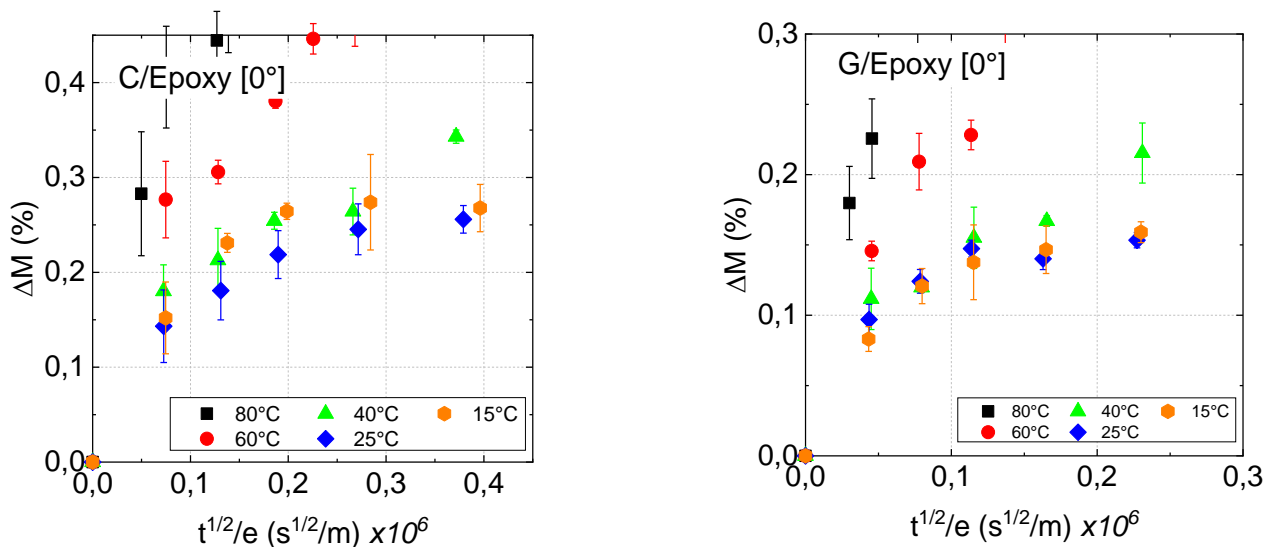


Figure 18: Temperature independent process in the first part of the sorption curves (a) Carbon/Epoxy (b) Glass/Epoxy

In these two figures shown in Figure 18, it is clear that an independent water diffusion process is observed in the early water absorption points, more especially at 40, 25 and 15°C. The reason why we are not observing the same phenomenon at 80 and 60°C may be due to the fact that the two water diffusion processes are competing within the same time range. This first independent water diffusion process was then

investigated more closely at 40, 25 and 15°C, by trying to describe it using a Fickian law. Results are shown for carbon and glass in Figure 19.

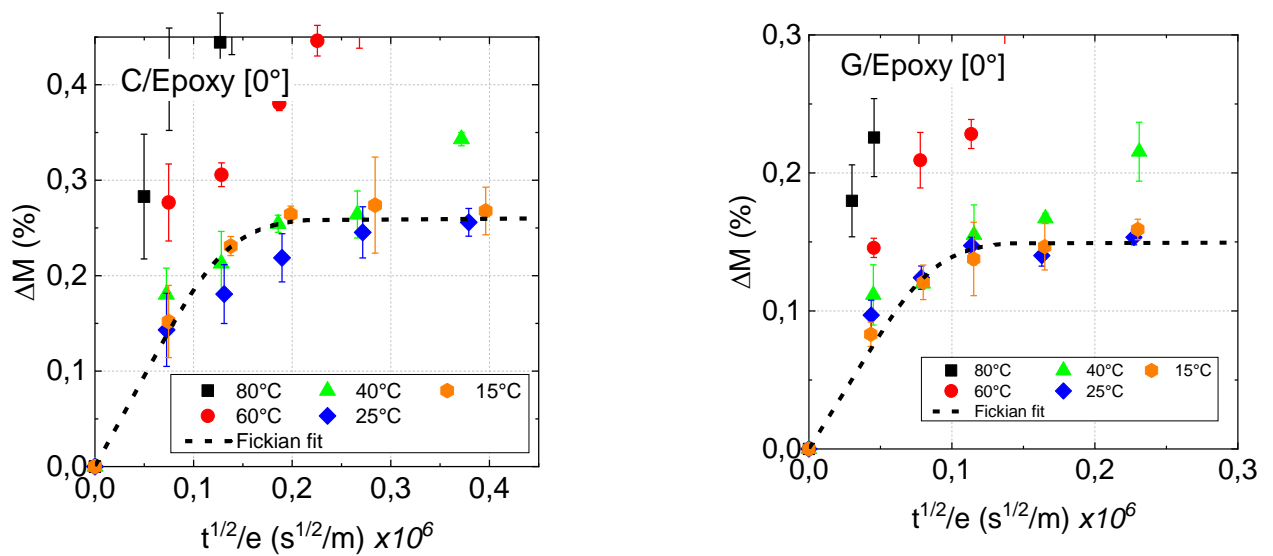


Figure 19: Temperature independent process in the first part of the sorption curves together with a Fickian description (a) Carbon/Epoxy (b) Glass/Epoxy

These results show that at 40, 25 and 15°C, this process is accurately described using a Fickian law using the water diffusion parameters shown in Table 5.

Table 5: Water diffusion parameters for the first water diffusion process in the composite

Material	$M_{\infty}$ (%)	D (m <sup>2</sup> /s)
Carbon/Epoxy	0.26	$1.1 \cdot 10^{-11}$
Glass/Epoxy	0.15	$3.36 \cdot 10^{-11}$

Then the second sorption process on the plots can be described using a Fickian law that depends on the temperature, Figure 20.

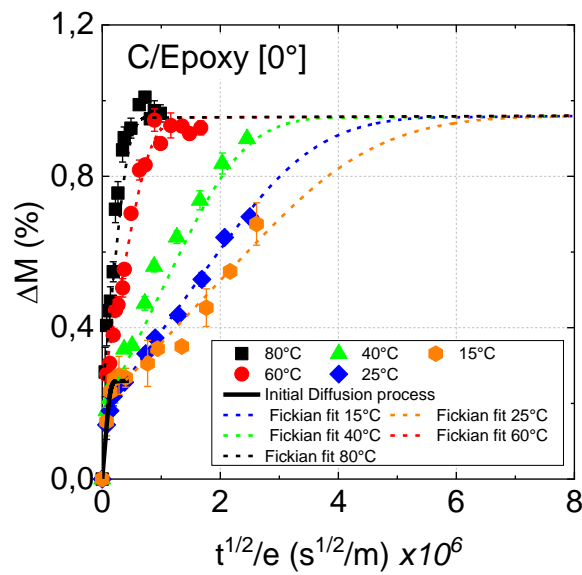


Figure 20: Water sorption processes in the carbon/epoxy composites immersed at different temperatures and associated modelling

The associated water diffusion coefficients at different temperatures are given in Table 6.

Table 6: Water diffusion parameters for the carbon/epoxy composites at different temperature

Temperature (°C)	D (m <sup>2</sup> /s)
80	5.52.10 <sup>-13</sup>
60	2.64.10 <sup>-13</sup>
40	2.73.10 <sup>-14</sup>
25	1.12.10 <sup>-14</sup>
15	1.05.10 <sup>-14</sup>

In a similar way to Figure 16, the water diffusion coefficients in the carbon/epoxy composites are plotted as a function of 1/RT in Figure 21.

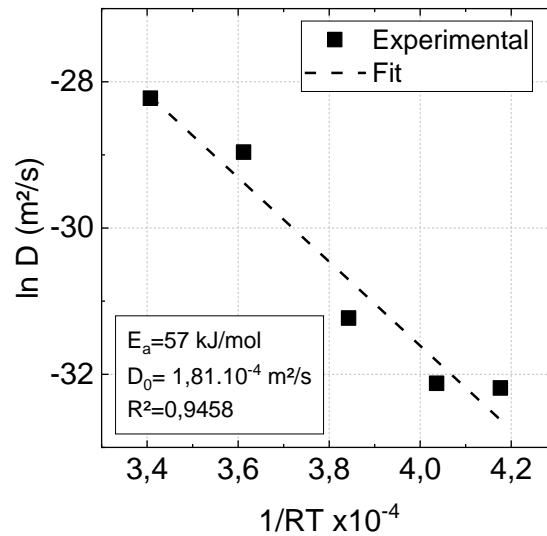


Figure 21: Measured diffusion coefficient D as a function of 1/RT on the carbon/epoxy composites

It may be noted that the activation energy for the composites is very close to that of the neat resin (57 kJ/mol for the composites and 61 kJ/mol for the resin). Results for the glass/epoxy composites are not shown here but results are very similar to those for the carbon/epoxy.

#### 4.2.2 Effect of stacking sequence on water absorption

The effect of stacking sequence is investigated in this section. For both the glass and carbon/epoxy composites, water saturation was reached for the specimens immersed at 60°C. Therefore, only the results from samples immersed at 60°C are discussed. These are presented in Figure 22.

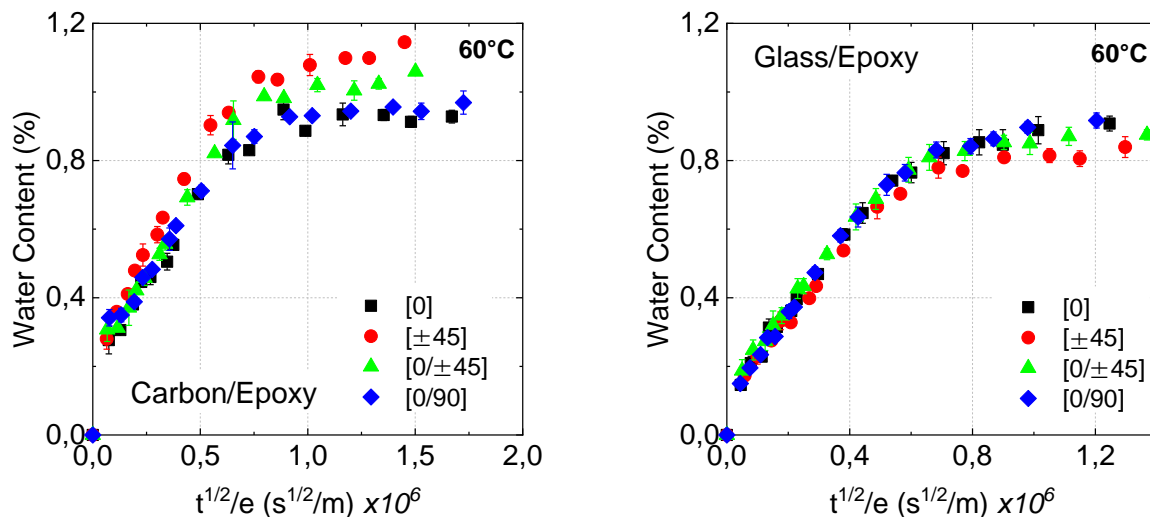


Figure 22: Effect of stacking sequence on the water diffusion for (a) Carbon/Epoxy (b) Glass/Epoxy

From these plots, results show that the stacking sequence has no effect on the glass/epoxy composites. A slight effect is observed on the carbon/epoxy composites, more especially the ones that

contain plies oriented at  $\pm 45^\circ$ . However, if we only take into account the water diffusion within the resin, i.e. if we remove the fibres from the equation (it is considered that the fibres do not absorb any water). The fibre weight content contained within the different composite panels are found in Table 7.

**Table 7: Fibre weight contents of the different panels**

Material	Carbon/Epoxy				Glass/Epoxy			
Sequence	[0]	$[\pm 45]$	$[0/\pm 45]$	$[0/90]$	[0]	$[\pm 45]$	$[0/\pm 45]$	$[0/90]$
$M_f$ (%)	$70.3 \pm 0.5$	$61.8 \pm 2.1$	$66.4 \pm 0.1$	$69.8 \pm 0.2$	$71.3 \pm 0.4$	$72.3 \pm 0.2$	$71.6 \pm 0.6$	$70.6 \pm 0.5$

Water sorption plots where only the water diffusion within the resin is considered is shown in Figure 23.

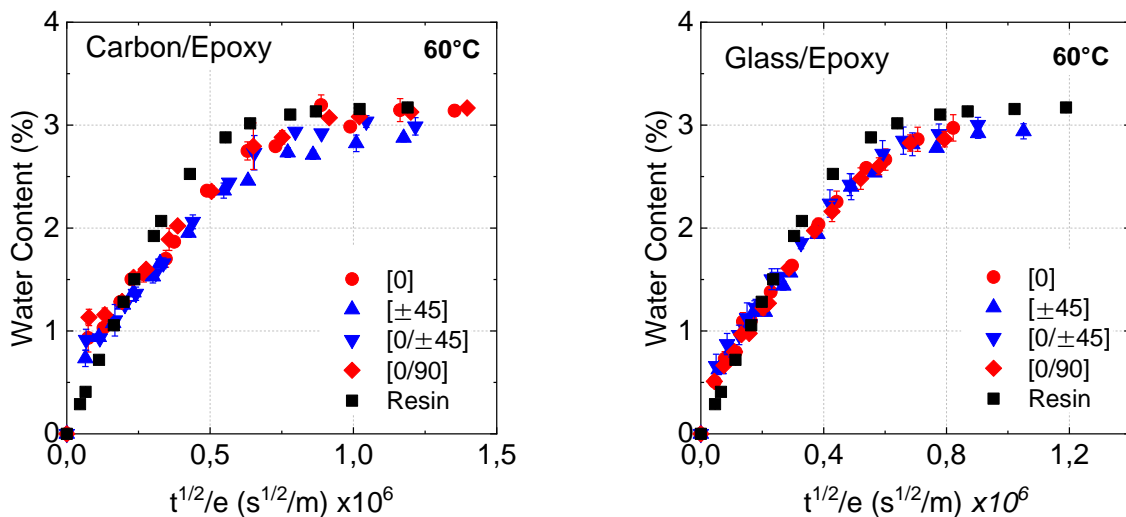


**Figure 23: Water diffusion within the resin only (a) Carbon/Epoxy (b) Glass/Epoxy**

Results from Figure 23 show that if we only consider the water diffusion within the resin, the stacking sequence does not have an effect on the water content at saturation. This means that the slight differences observed on Figure 22 only depend on the fibre weight content. Therefore, the stacking sequence does not have a significant effect on the water content at saturation.

#### 4.2.3 Desorption at 60°C

Finally, the water desorption process after aging was investigated and results are shown in Figure 24 for the carbon/epoxy composites. Results for the glass/epoxy are not presented here. The glass/epoxy composites were thicker than those made of carbon, so the time needed to reach the water saturation was much longer and stabilization has not yet been reached.

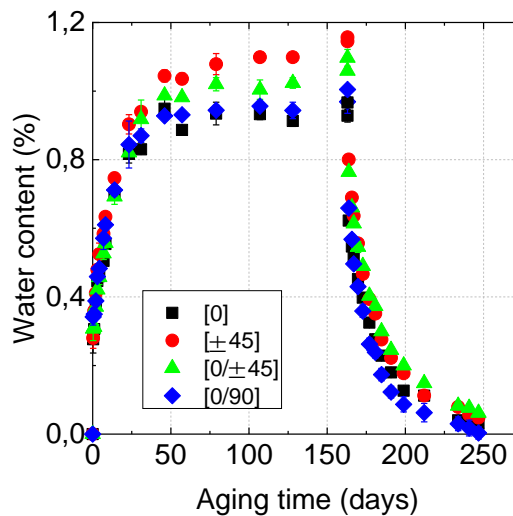


Figure 24: Desorption process on the carbon/epoxy composites, 60°C

Results from Figure 24 show that after the desorption process, the mass of the different samples return to their initial unaged mass. This suggests no degradation during sea water aging.

### 4.3 Conclusion

This section was devoted to the water diffusion kinetics within the neat resin and the composites, both carbon and glass. The aim of this section was to investigate whether or not water diffusion modelling was possible and if the different stacking sequences in the composites had an effect on the water content at saturation.

First, results showed that the water diffusion within the resin was accurately described at different temperatures by the means of a Fickian description and an Arrhenius approach.

Second, the water diffusion within the composite materials was investigated. Results have shown that the stacking sequence did not have an effect on the water content at saturation. Then, results have shown that the water diffusion within these materials followed a two-step process. A first water diffusion process independent of the water temperature was observed in the early stage of the sorption curve. Then, a second water diffusion process was described using an Arrhenius approach similar to that of the resin.

All these results show that we are able to model the water diffusion within the materials of the study. Finally, these results show that accelerated aging is necessary in such a study and for such applications. After one year of aging, the 2 mm thick specimens immersed at 15°C are still not fully saturated. Based on the water diffusion coefficients determined here at 15°C, the 2 mm thick specimens would be fully saturated after 2.5 years of water immersion, which is too long if we take into account the length of the project.

Also, the thinnest part of the D12 blade is about 20 mm. If we were to immerse such a thick specimen in sea water at 15°C, it would take more than 250 years to fully saturate the blade, which again justifies an accelerated study on thin specimens.

## 5. MECHANICAL TESTS - STATIC PROPERTIES

This section is devoted to the determination of the static properties needed for blade design, both in the unaged state and after sea water aging. First, a short section describes the properties that are needed for blade design. If we consider a unidirectional composite material with three principal directions 1, 2 and 3, as shown in Figure 25, the engineering constants to be determined are presented in the equation hereafter.

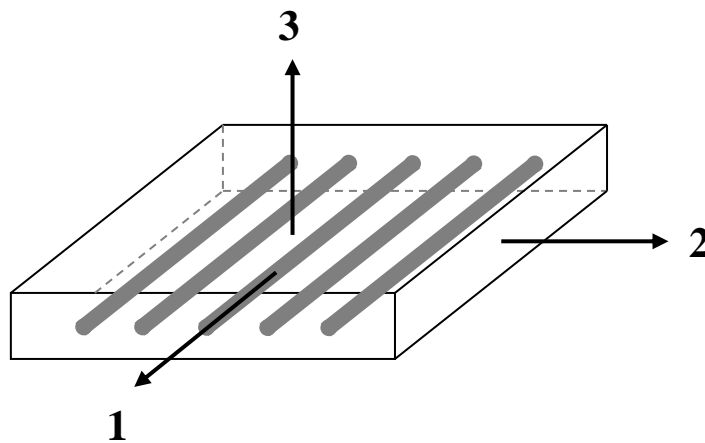


Figure 25: Schematic representation of a transversely isotropic composite material

$$\begin{Bmatrix} \varepsilon_1 \\ \varepsilon_2 \\ \varepsilon_3 \\ \varepsilon_4 \\ \varepsilon_5 \\ \varepsilon_6 \end{Bmatrix} = \begin{bmatrix} 1/E_1 & -\nu_{21}/E_2 & -\nu_{31}/E_3 & 0 & 0 & 0 \\ -\nu_{12}/E_1 & 1/E_2 & -\nu_{32}/E_3 & 0 & 0 & 0 \\ -\nu_{13}/E_1 & -\nu_{23}/E_2 & 1/E_3 & 0 & 0 & 0 \\ 0 & 0 & 0 & 1/G_{23} & 0 & 0 \\ 0 & 0 & 0 & 0 & 1/G_{31} & 0 \\ 0 & 0 & 0 & 0 & 0 & 1/G_{12} \end{bmatrix} \begin{Bmatrix} \sigma_1 \\ \sigma_2 \\ \sigma_3 \\ \sigma_4 \\ \sigma_5 \\ \sigma_6 \end{Bmatrix}$$

From this, we need to determine all the stiffness related properties, i.e.  $E_1, E_2, E_3, G_{12}, G_{31}, G_{23}, \nu_{12}, \nu_{13}, \nu_{23}, \nu_{21}, \nu_{31}, \nu_{32}$ , so 12 independent properties. However, composite materials are usually considered to be transversely isotropic, which reduces the number of elastic constants to be determined:  $E_1; E_2=E_3; G_{12}=G_{13}; G_{23} = \frac{E_{23}}{2(1+\nu_{23})}; \nu_{23}; \nu_{12}=\nu_{13}; \frac{\nu_{ij}}{E_i} = \frac{\nu_{ji}}{E_j}$

Finally, for most composite materials, 4 in-plane stiffness related properties are needed,  $E_1, E_2, G_{12}$ , and  $\nu_{12}$ . To determine these, tensile tests on composite specimens are performed on three different sequences: [0], [90] and [ $\pm 45$ ], shown in Figure 26.

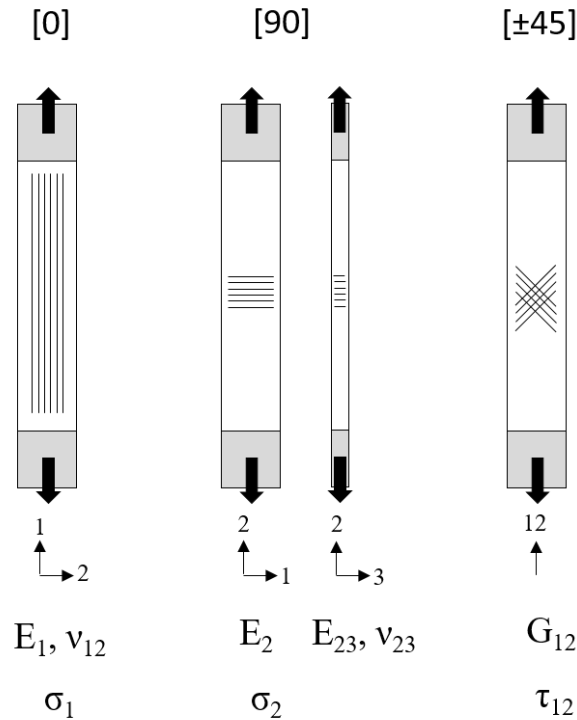


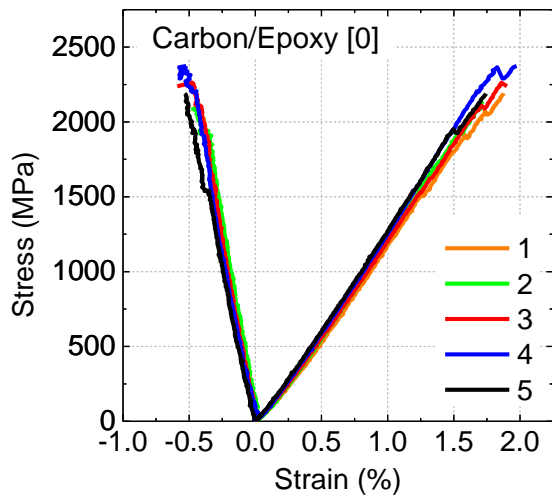
Figure 26: Tensile tests performed to determine input data for blade design

Therefore tests were performed within RealTide on these specific but essential stacking sequences. It may be noted that  $E_{23}$  and  $\nu_{23}$  were not determined due to the thickness of the laminates investigated here (2 mm thick). It is indeed difficult to obtain accurate data on such thin laminates. Nonetheless, these can be approximated using data from the literature.

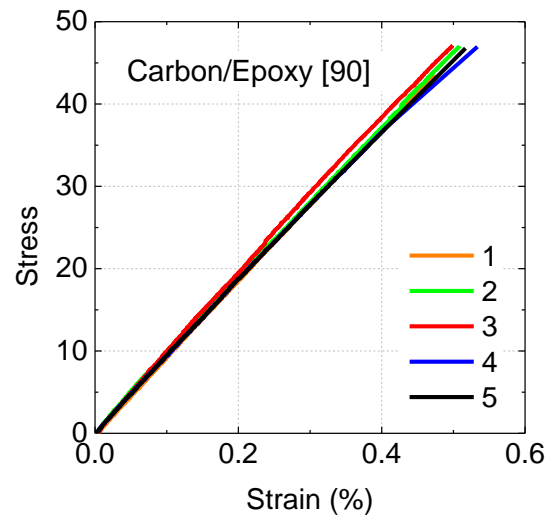
## 5.1 Static properties in the unaged state

### 5.1.1 Tensile tests

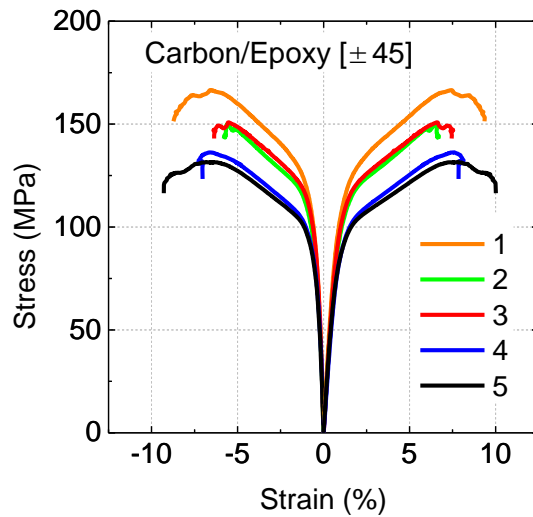
Results from tensile tests are shown in this section. First, results concerning the carbon/epoxy composites are presented. Results from tensile tests performed on the unidirectional carbon/epoxy (P1) in the longitudinal [0] and transverse [90] directions are respectively shown in Figure 27a and Figure 27b. Results from in-plane shear tests (P2) are shown in Figure 27c.



(a)



(b)



(c)

Figure 27: Stress-strain plots for carbon/epoxy (a) P1 - [0] (b) P1 - [90] (c) P2 - [±45]

For each test presented in Figure 27, the failures were valid and occurred at the centre of the specimen, as presented in Figure 28.

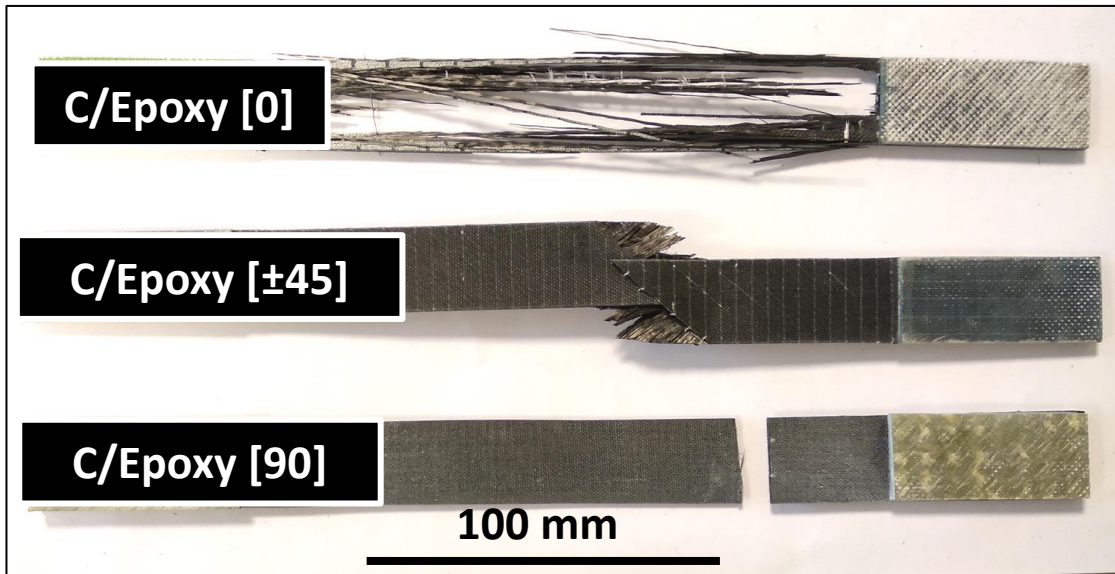
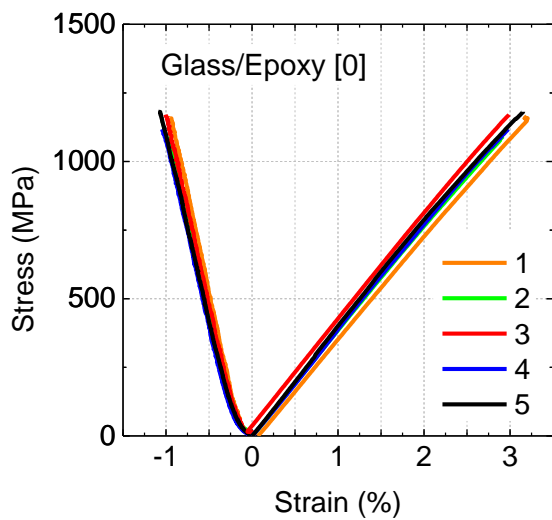
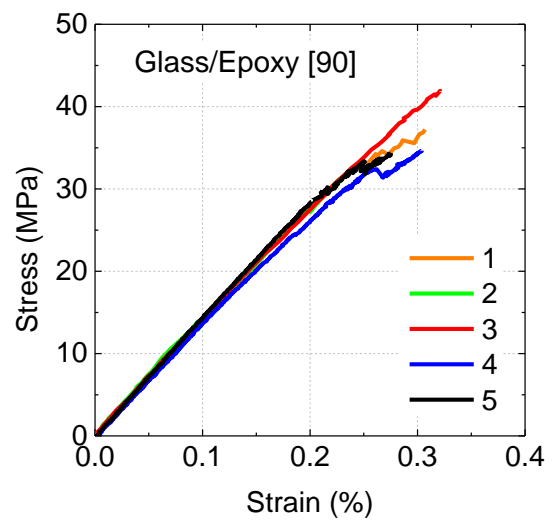


Figure 28: Valid failure modes obtained on the Carbon/Epoxy specimens

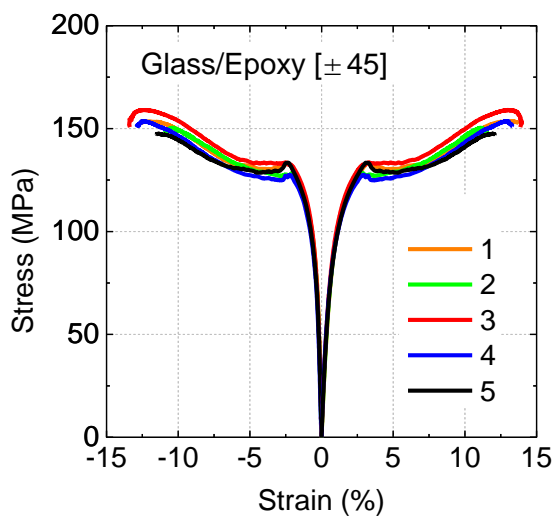
The same tests were performed on the glass/epoxy composites. Results from those performed on the unidirectional glass/epoxy (P5) in the longitudinal [0] and transverse [90] directions are respectively shown in Figure 29.a and Figure 29.b. Results from in-plane shear tests (P6) are shown in Figure 29.c.



(a)



(b)



(c)

Figure 29: Stress-strain plots for carbon/epoxy (a) [0] (b) [90] (c) [±45]

Again, for each tensile test performed here, the failures occurred in the central part of the specimen, Figure 30.

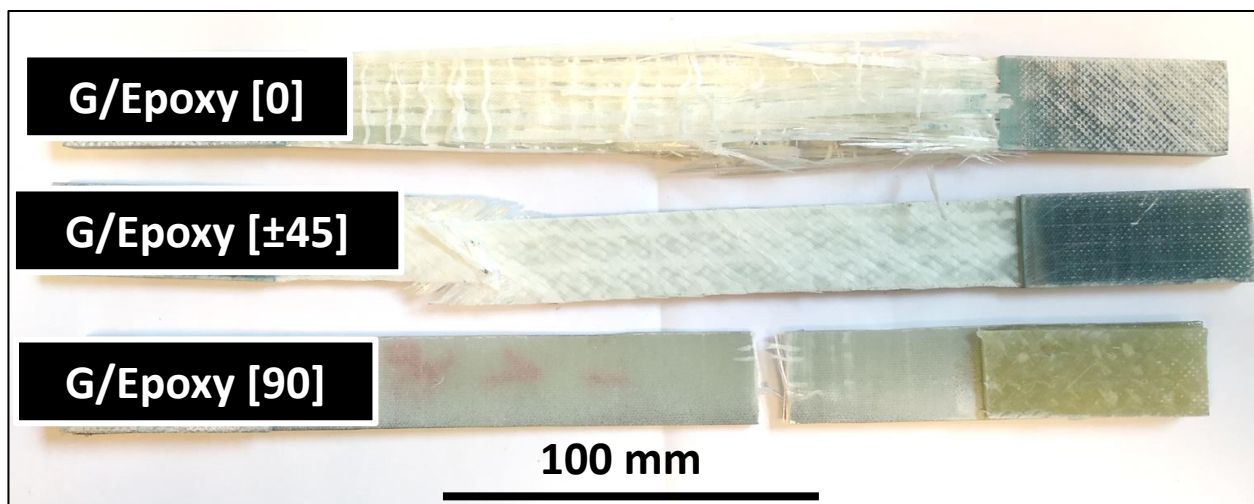


Figure 30: Valid failure modes obtained on the Glass/Epoxy specimens

The neat resin has also been tested in tension. Results are shown in Figure 31.

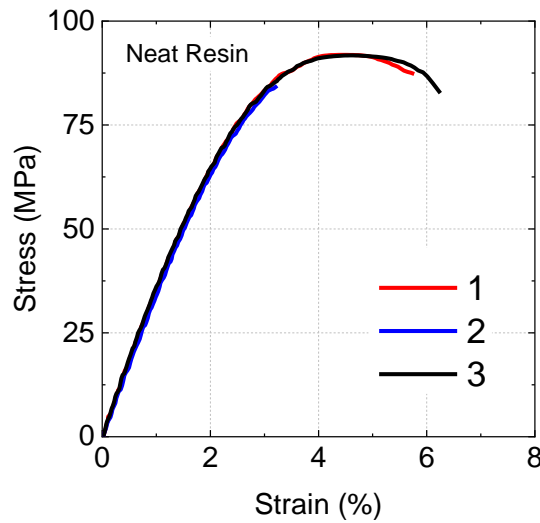


Figure 31: Tensile tests on the unaged resin

Finally, the data from all the tests that have been performed here are summarized in Table 8. This table contains the data needed for modelling and design. It may be noted that the data presented here are in accordance with published results for similar carbon and glass/epoxy composites.

Table 8: Material properties determined in this report for carbon/epoxy and glass/epoxy

Material	C/Epoxy	G/Epoxy
$E_1$ (GPa)	$120.3 \pm 2.1$	$42.3 \pm 3.6$
$E_2$ (GPa)	$9.4 \pm 0.3$	$14.1 \pm 0.3$
$G_{12}$ (GPa)	$4.5 \pm 0.4$	$5.4 \pm 0.3$
$\nu_{12}$	$0.26 \pm 0.02$	$0.34 \pm 0.03$
$\sigma_1$ (MPa)	$2285 \pm 102$	$1148 \pm 43$
$\sigma_2$ (MPa)	$46 \pm 2$	$36 \pm 4$
$\tau_{12}$ (MPa)	$73 \pm 7$	$76 \pm 2$
$\tau_{13}$ (MPa)	$72 \pm 2$	$52 \pm 3$
$E_{resin}$ (GPa)	$3.6 \pm 0.1$	
$\sigma_{resin}$ (MPa)	$92 \pm 1$	

### 5.1.2 Interlaminar Shear Strength tests (ILSS)

Results from apparent Interlaminar Shear Strength in the unaged state are shown in this section. First, the stress-displacement plots for unidirectional glass/epoxy and carbon/epoxy composites are respectively shown in Figure 32.a and Figure 32.b.

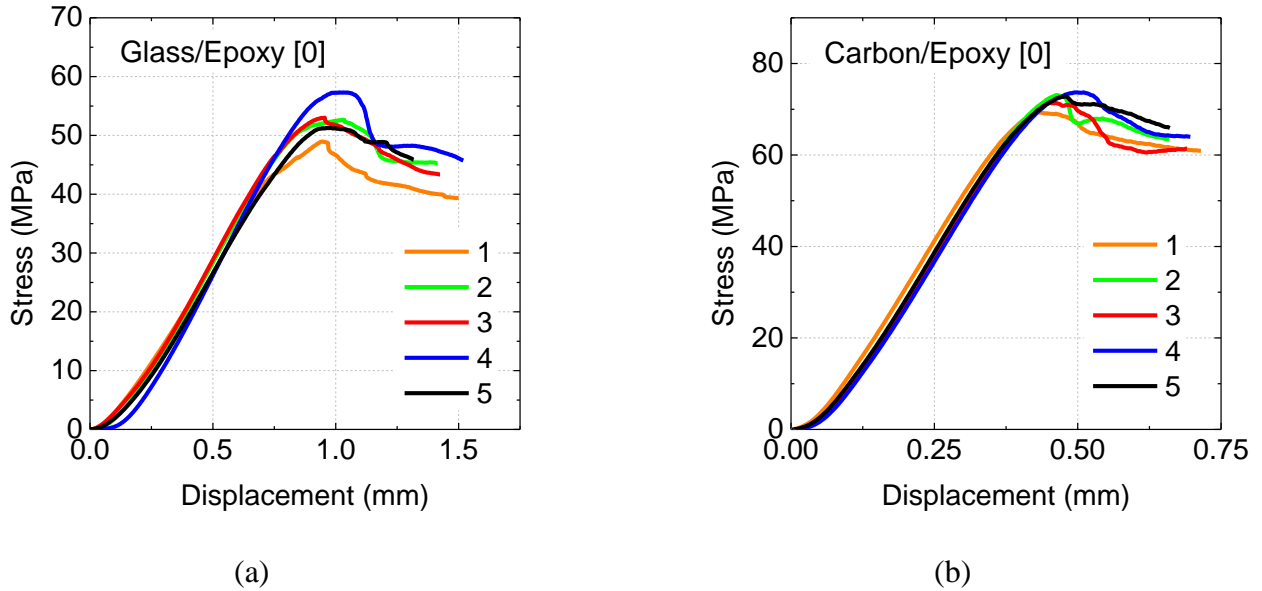


Figure 32: Plots obtained from ILSS tests on the 0/90 specimens (a) Glass/epoxy (b) Carbon/Epoxy

Stress values at failure are now summarized in Table 9.

Table 9: Results from ILSS tests

Material	Composite	Sequence	$\tau_{13}$ (MPa)
C/Epoxy	P1	[0]	$72 \pm 2$
G/Epoxy	P5	[0]	$52 \pm 3$

These results show that the interlaminar shear strength for the carbon/epoxy composite is 30% higher than that of the glass/epoxy composite. However, in both cases, the interlaminar shear strength is above 50 MPa, which indicates that the interface between fibre and matrix is of good quality.

### 5.1.3 Flexural properties

Results from flexural tests performed on the carbon/epoxy laminates are shown in Figure 33 and those performed the glass/epoxy laminates in Figure 34. Results are then summarized in Table 10.

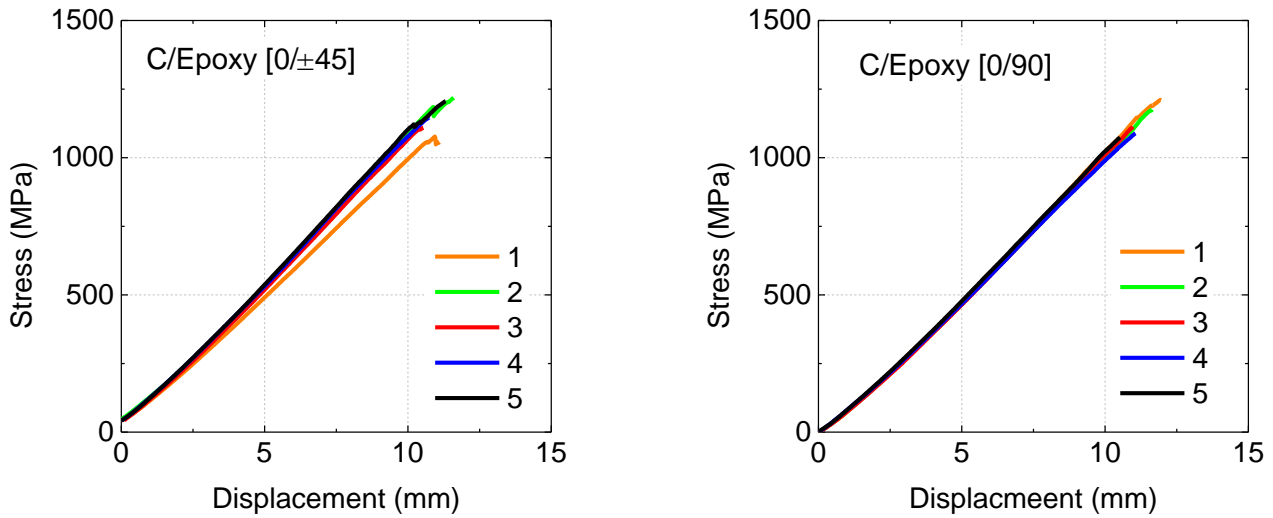


Figure 33: Static flexural tests performed on the carbon/epoxy laminates (a) [0/±45] (b) [0/90]

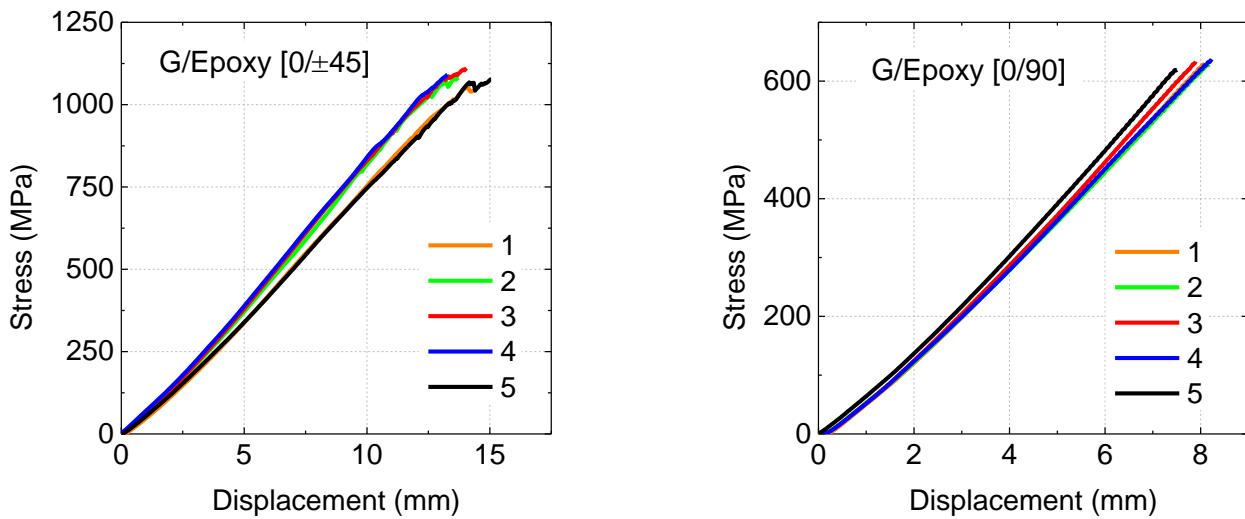


Figure 34: Static flexural tests performed on the glass/epoxy laminates (a) [0/±45] (b) [0/90]

Table 10: Results from flexural tests in the unaged state

Material	Composite	Sequence	$\sigma_{failure}$ (MPa)
C/Epoxy	P3	[0/±45]	1151 ± 61
	P4	[0/90]	1132 ± 58
G/Epoxy	P7	[0/±45]	1083 ± 21
	P8	[0/90]	630 ± 7

Results show that for the carbon/epoxy laminates, the flexural strength is above 1000 MPa. This confirms that these laminates are of very good quality. Concerning the glass/epoxy laminates, the [0/±45] specimens broke at flexural strength values above 1000 MPa but the [0/90] laminates broke around 600 MPa. This difference may be explained by a poorer interface quality.

## 5.2 Static properties in sea water in the saturated state

The following section is devoted to the effect of sea water absorption on the mechanical properties of carbon and glass/epoxy composites. The neat resin is also investigated.

The aim of this section is to investigate which of the two materials (carbon or glass) is more suitable for tidal applications based on the results from sea water aging.

First, it was shown in section 4 that all three materials (neat resin, carbon/epoxy and glass/epoxy) absorb water while immersed in sea water. This water absorption process induces a phenomenon called plasticization, which induces a decrease in the glass transition temperature, as shown in Figure 35. Results from DSC show that the glass transition temperature decreases from 95°C to 78°C. It is important to check the value of  $T_g$  after water saturation, as if it drops below the immersion water temperature additional (non-representative) aging mechanisms may occur as the matrix will be in the rubbery state. The specimens aged in this study were all aged below the glass transition temperature.

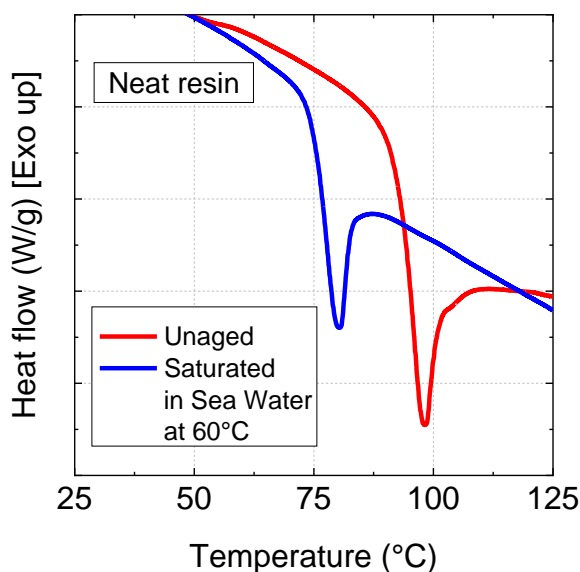


Figure 35: Decrease in  $T_g$  with water absorption within the neat resin (DSC)

### 5.2.1 Tensile tests

Results from tensile tests performed after sea water aging on the neat resin, carbon/epoxy and glass/epoxy composites are respectively shown in Figure 36, Figure 37 and Figure 38. Results from these tests are summarized in Table 11.

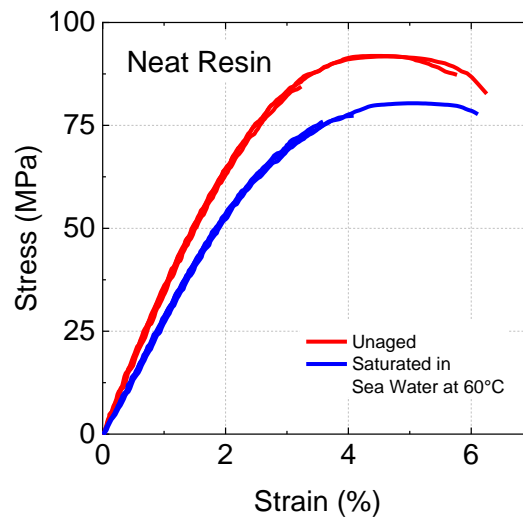
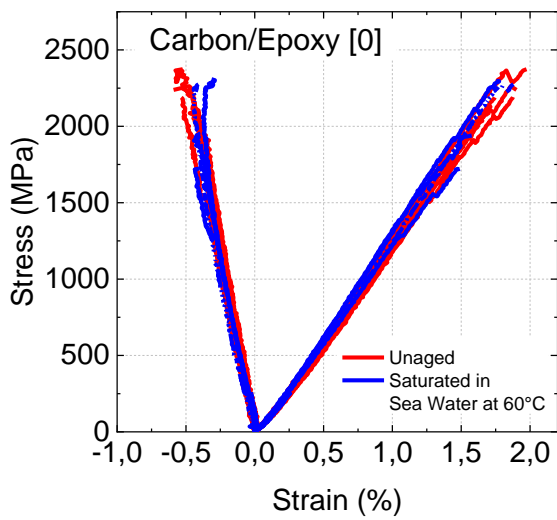
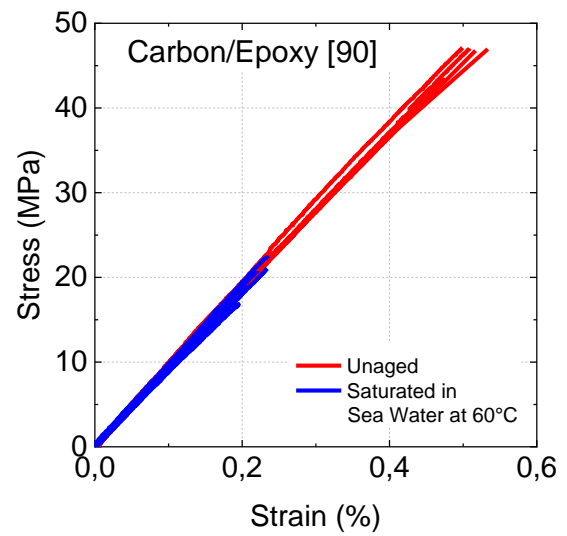


Figure 36: Effect of sea water absorption on the tensile properties of the neat resin

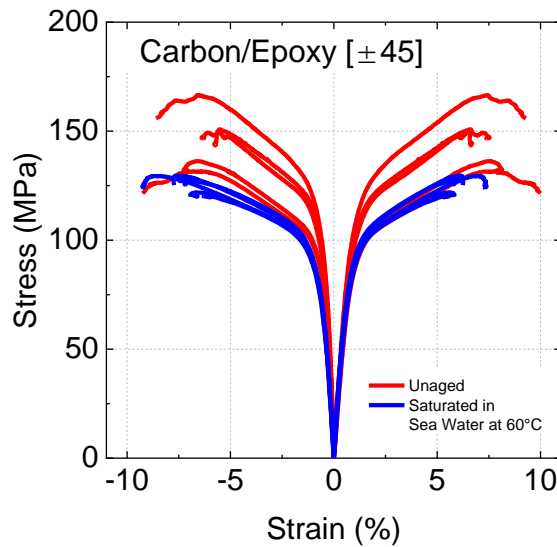
Results from tensile tests performed on the neat resin after aging show that there is a decrease of about 20% in both the maximal stress and the modulus. This corresponds to the plasticization mechanism.



(a)



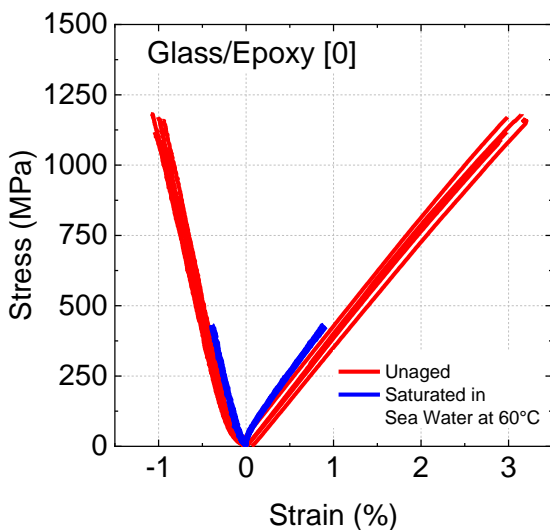
(b)



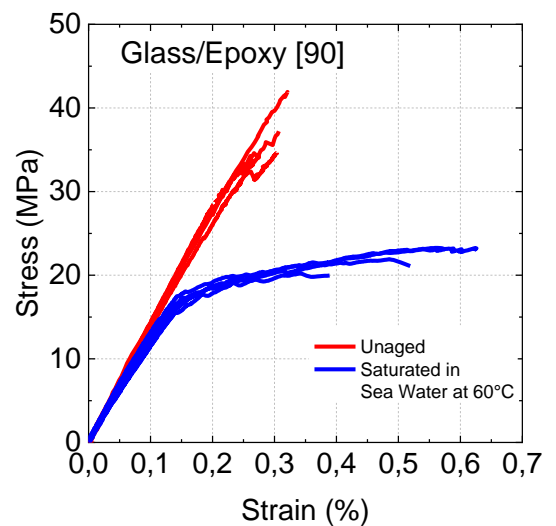
(c)

Figure 37: Effect of sea water absorption on the tensile properties of the carbon/epoxy laminates (a) [0°] (b) [90°] (c) [±45°]

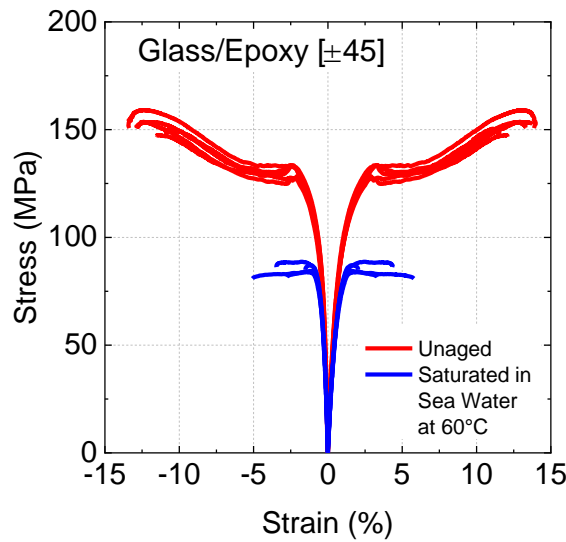
A decrease in the stress at break is observed after sea water aging when the composite is tested along a matrix-dominated direction, i.e. for the [90°] and [±45°] sequences. No effect is observed on the fibre-dominated properties [0°]. While a 20% decrease in the properties on the [±45°] specimens is consistent with results from the resin after aging, a decrease of more than 50% on the [90°] specimens is unexpected and suggests a degradation of the interface during sea water aging. However, the effect of water absorption on the modulus is quite small.



(a)



(b)



(c)

Figure 38: Effect of sea water absorption on the tensile properties of the glass/epoxy laminates (a) [0] (b) [90] (c) [±45]

Results from tests performed on the glass/epoxy composites after aging all resulted in a significant decrease in the mechanical properties. This is true for most properties, but more especially for the stress at break, which decreases by more than 50% for all tests, even for fibre-dominated tests. This suggests a significant degradation of the interface and the fibres. The failure mode was also modified for the [0] tests as it was no longer characterised by fibre splitting, the failure mode usually noted on unidirectional specimens tested under tension. This is shown in Figure 39.

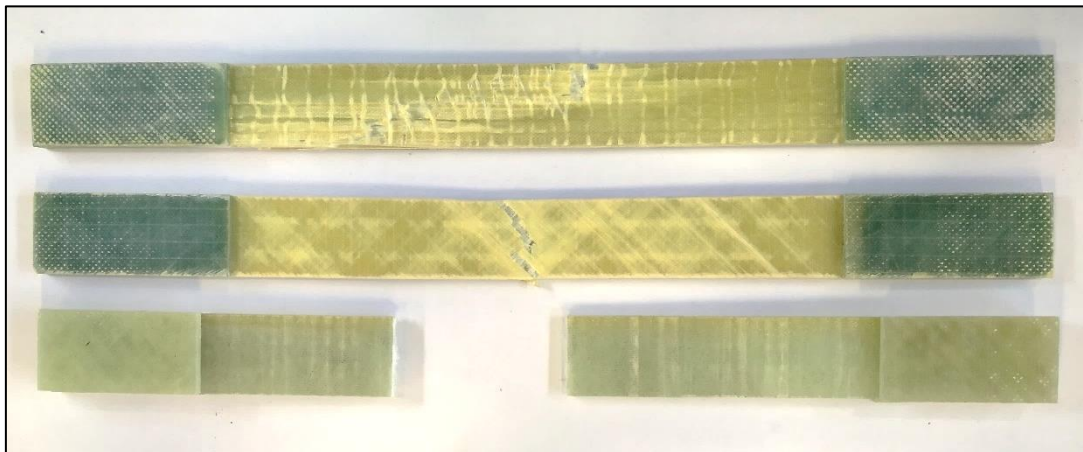


Figure 39: Failure mode of glass/epoxy specimens tests in tension – Top specimen [0], mid specimen [±45], bottom specimen [90]

Table 11: Results from tensile tests performed after sea water aging

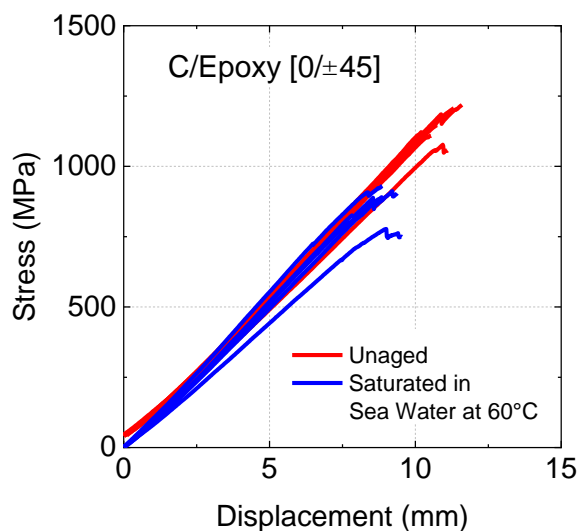
Material	C/Epoxy	G/Epoxy	C/Epoxy	G/Epoxy
Condition	Unaged	Unaged	Saturated in Sea Water at 60°C	Saturated in Sea Water at 60°C

$E_1$ (GPa)	$120.3 \pm 2.1$	$42.3 \pm 3.6$	$121.1 \pm 3.6$	$43.0 \pm 0.9$
$E_2$ (GPa)	$9.4 \pm 0.3$	$14.1 \pm 0.3$	$9.4 \pm 0.5$	$11.8 \pm 0.5$
$G_{12}$ (GPa)	$4.5 \pm 0.4$	$5.4 \pm 0.3$	$3.4 \pm 0.1$	$3.5 \pm 0.1$
$\nu_{12}$	$0.26 \pm 0.02$	$0.34 \pm 0.03$	$0.25 \pm 0.05$	$0.34 \pm 0.01$
$\sigma_1$ (MPa)	$2285 \pm 102$	$1148 \pm 43$	$2083 \pm 102$	$420 \pm 18$
$\sigma_2$ (MPa)	$46 \pm 2$	$36 \pm 4$	$20 \pm 2$	$17 \pm 1^*$
$\tau_{12}$ (MPa)	$73 \pm 7$	$76 \pm 2$	$63 \pm 2$	$43 \pm 1$
$\tau_{13}$ (MPa)	$72 \pm 2$	$52 \pm 3$	$59 \pm 2$	$34 \pm 3$
$E_{resin}$ (GPa)	$3.6 \pm 0.1$		$2.8 \pm 0.1$	
$\sigma_{resin}$ (MPa)	$92 \pm 1$		$78 \pm 2$	

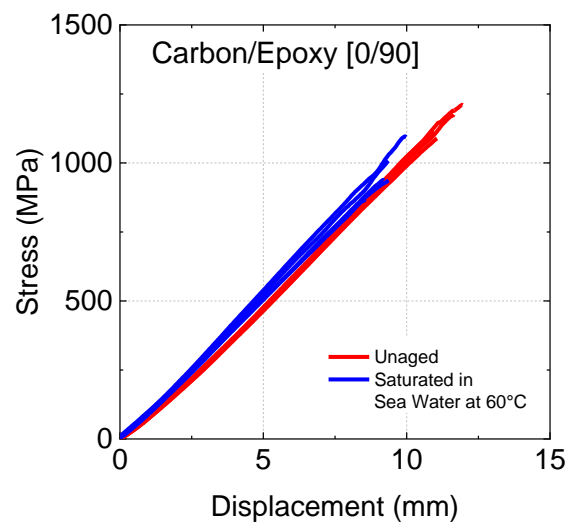
Results from these tests performed after aging showed that the glass/epoxy composites were much more sensitive to sea water aging than their carbon fibre reinforced counterparts.

### 5.2.2 Flexural properties

Results from four point bending tests performed after sea water aging are shown in Figure 40 and Figure 41 for both carbon and glass, respectively.



(a)



(b)

Figure 40: Static flexural tests performed on the carbon/epoxy laminates after aging (a) [0/±45] (b) [0/90]

For both carbon/epoxy sequences tested here after aging, the flexural strength decreases by about 20%.

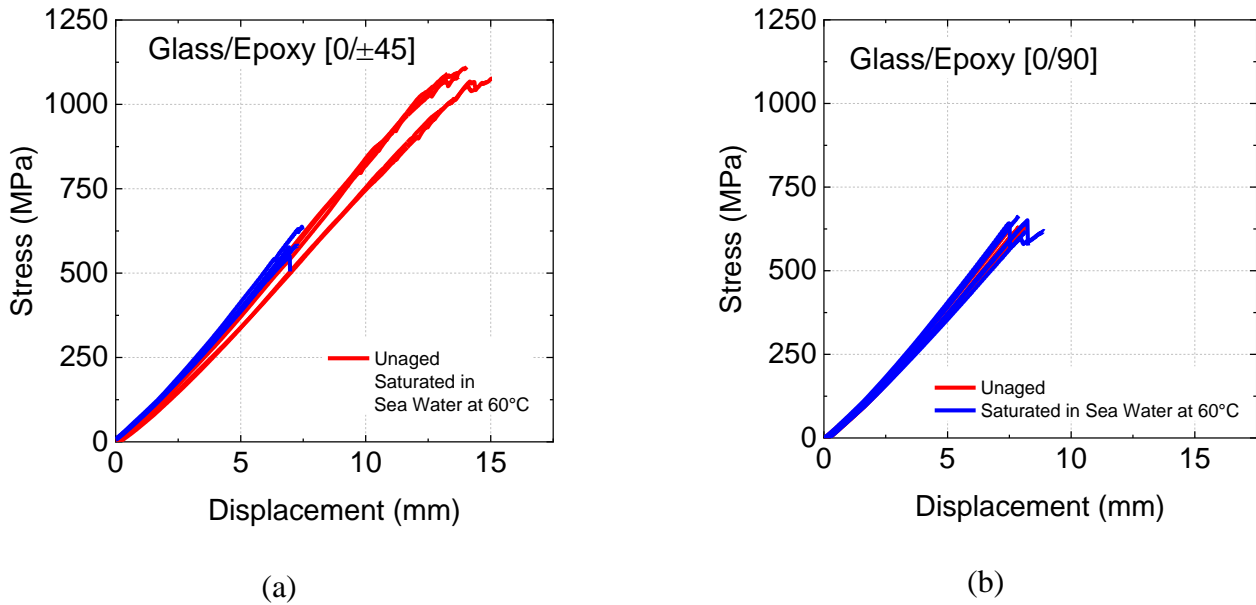


Figure 41: Static flexural tests performed on the glass/epoxy laminates after aging (a) [0/±45] (b) [0/90]

On the other hand, results for the glass/epoxy composites tested after aging are quite different. A decrease of about 50% on the flexural strength is observed for the [0/±45] sequence. This is associated with a change in the failure mode from compression failures in the unaged state to tensile failures after aging, as shown in Figure 42.

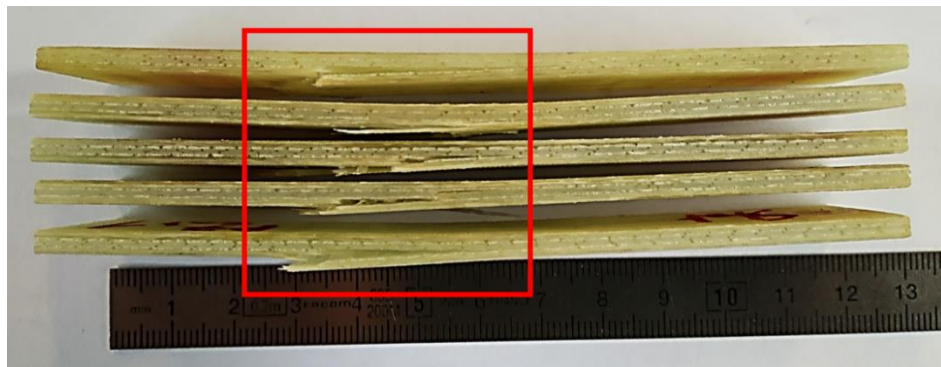


Figure 42: Tensile failure mode on the [0/±45] glass/epoxy composites after aging

Similarly to the results shown in the previous section, this suggests a significant degradation of the fibre/matrix interface induced by aging. No decrease is observed on the [0/90] sequence. Nonetheless, it was suggested in section 5.1.3 that the interface was of a poor quality on this sequence, as it failed at a much lower flexural stress level. Finally, both sequences fail at the same flexural strength value after aging, around 600 MPa, which is much lower than the carbon/epoxy composite after aging (around 900 MPa), see Table 12.

**Table 12: Results from flexural tests performed after sea water aging**

Material	Sequence	$\sigma_{\text{failure}}$ (MPa)	
		Unaged	Saturated in Sea Water at 60°C
C/Epoxy	[0/±45]	1151 ± 61	879 ± 60
	[0/90]	1132 ± 58	969 ± 87
G/Epoxy	[0/±45]	1083 ± 21	582 ± 33
	[0/90]	630 ± 7	642 ± 17

### 5.2.3 Conclusion

Results presented in this section highlighted that sea water aging can have a significant effect on the mechanical properties. This has been observed on the three materials investigated here, i.e. the neat resin as well as carbon and glass/epoxy composites. While some properties decreased by about 20% due to plasticization (reversible effect if water when removed from the material), interface degradation upon aging was suggested many times. This suggests that irreversible degradation occurred. Therefore, it is expected that if water is removed from these materials after aging (desorption), most of the initial unaged properties will not be recovered. This is examined in more detail in the following section.

Finally, it was shown that aging has a more important impact on the glass/epoxy composites than the carbon/epoxy composites. Therefore, based on these results, the carbon/epoxy composite appears more suitable for tidal applications.

### 5.3 Static properties after water desorption

This section investigates whether or not the decrease in mechanical properties observed in the previous section is reversible when water is removed from the materials by drying. It was stated in section 4.2.3 that water absorption was fully reversible in terms of water content (Figure 24) on the carbon/epoxy specimens, but not on the neat resin, which was unexpected.

First, results from tensile tests after the desorption process on the neat resin are shown in Figure 43. These results show that the sea water aging process is mostly reversible. A slight difference compared to the unaged material is observed, and may be associated with oxidation on the surface of the specimens.

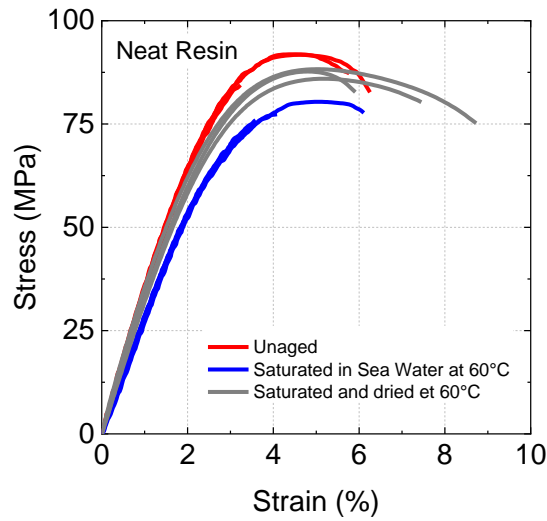
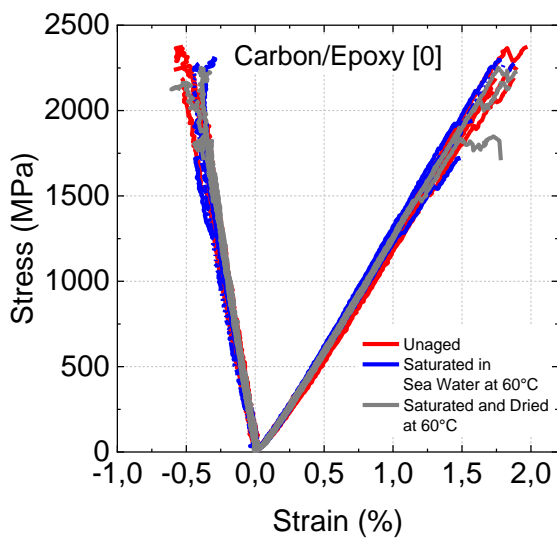
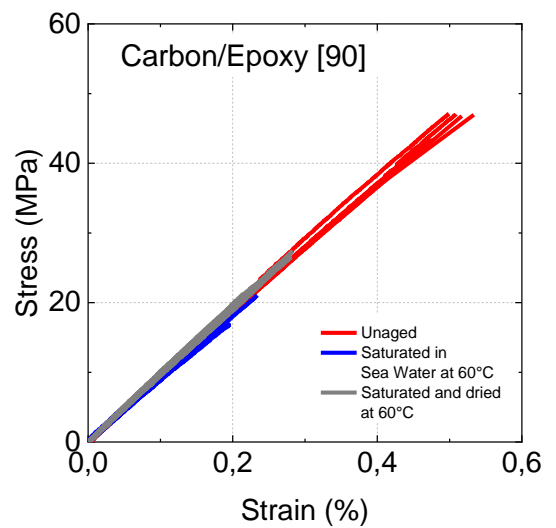


Figure 43: Effect of water desorption after aging on the tensile properties of the neat resin

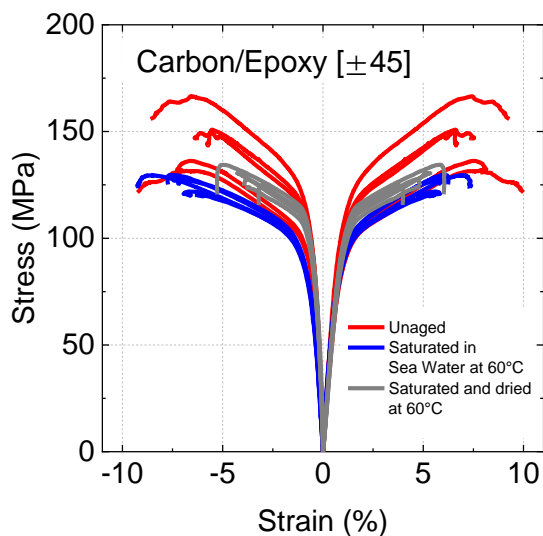
Then, results from tensile tests performed after the desorption process on the carbon/epoxy composites are shown in Figure 44. Results show that after drying, the mechanical properties are not recovered, particularly for the 90° tests. This suggests a degradation of the interface coupled with a slight oxidation of the resin. The mechanical properties are summarized in Table 13.



(a)



(b)



(c)

Figure 44: Effect of water desorption after aging on the tensile properties of the carbon/epoxy laminates (a) [0] (b) [90] (c) [±45]

Table 13: Results from tensile tests performed on the carbon/epoxy in the unaged, aged and dried after aging states

Material	C/Epoxy	C/Epoxy	C/Epoxy
Condition	Unaged	Saturated in Sea Water at 60°C	Saturated then Dried at 60°C
$E_1$ (GPa)	$120.3 \pm 2.1$	$121.1 \pm 3.6$	$123.2 \pm 1.9$
$E_2$ (GPa)	$9.4 \pm 0.3$	$9.4 \pm 0.5$	$9.7 \pm 0.5$
$G_{12}$ (GPa)	$4.5 \pm 0.4$	$3.4 \pm 0.1$	$4.1 \pm 0.1$
$\nu_{12}$	$0.26 \pm 0.02$	$0.25 \pm 0.05$	$0.22 \pm 0.03$
$\sigma_1$ (MPa)	$2285 \pm 102$	$2083 \pm 102$	$2032 \pm 234$
$\sigma_2$ (MPa)	$46 \pm 2$	$20 \pm 2$	$25 \pm 2$
$\tau_{12}$ (MPa)	$73 \pm 7$	$63 \pm 2$	$64 \pm 2$
$\tau_{13}$ (MPa)	$72 \pm 2$	$59 \pm 2$	$62 \pm 4$
$E_{resin}$ (GPa)	$3.6 \pm 0.1$	$2.8 \pm 0.1$	$3.3 \pm 0.2$

$\sigma_{\text{resin}}$ (MPa)	$92 \pm 1$	$78 \pm 2$	$87 \pm 1$
-------------------------------	------------	------------	------------

14. Similar conclusions are reached on specimens tested under flexure after the desorption process, Table

**Table 14: Flexural properties after desorption on [0/±45] carbon/epoxy**

Condition	$\sigma_{\text{failure}}$ (MPa)
Unaged	$1151 \pm 61$
Saturated in Sea Water at 60°C	$879 \pm 60$
Saturated and Dried at 60°C	$1043 \pm 83$

## 6. MECHANICAL TESTS – FATIGUE PROPERTIES

Although static mechanical characterization in the aged state is of particular interest, a turbine blade during use is subjected to flexural fatigue loadings. This is one of the reasons why four point flexural fatigue tests were performed within REALTIDE on composite sequences likely to be used in design, such as [0/90]<sub>s</sub> and [0/±45]<sub>s</sub>, before and after sea water aging.

First, results from flexural fatigue tests in the unaged states are presented. This will provide a comparison between carbon and glass in the unaged state as well as a comparison between sequences for the same material (carbon/epoxy)

Then, results after sea water aging are presented, followed by results after water desorption.

### 6.1 Fatigue properties in the unaged state

#### 6.1.1 Comparison between carbon/epoxy laminates with different stacking sequences

First, results from flexural fatigue tests in the unaged state are shown in Figure 45. The aim is to compare results for two different sequences with the same material, i.e. carbon/epoxy. It should be remembered that for both sequences, the flexural strengths under static loading were very similar, around 1100 MPa. This partly explains why the fatigue curves on Figure 45 are very similar for both sequences. The most dominant failure mode for both sequences was delamination between the outer unidirectional ply and the inner [±45] or [90] plies.

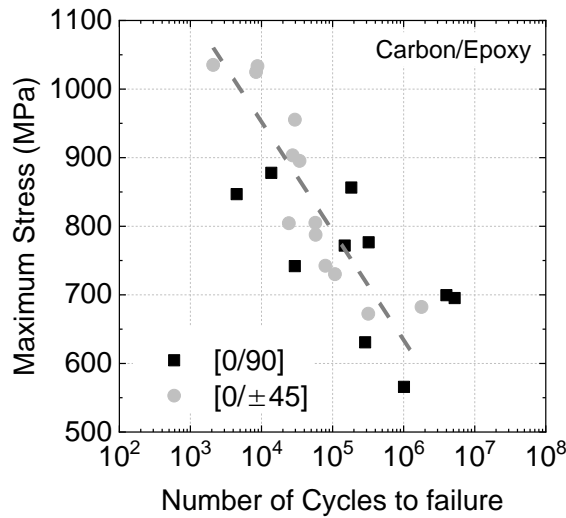


Figure 45: Flexural fatigue tests on carbon/epoxy laminates in the unaged state – Comparison between [0/45] and [0/90] sequences

### 6.1.2 Comparison between carbon/epoxy and glass/epoxy laminates with the same stacking sequence

Results presented in Figure 46 show flexural fatigue tests performed on two different materials, i.e. carbon and glass, but using the same stacking sequence [0/±45]. Unlike the results shown in Figure 45, the slopes of the fatigue curves are very different. Therefore, there is a clear effect of material system on the flexural fatigue life, even though the static strengths were very similar. From these results, it is clear that such glass/epoxy composites do not perform as well as carbon/epoxy in the unaged state.

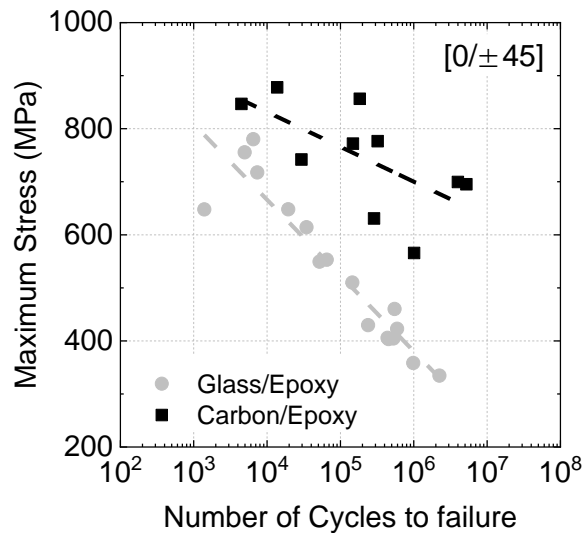


Figure 46: Flexural fatigue tests in the unaged state – Comparison between glass and carbon

## 6.2 Fatigue properties in the aged state

Results from flexural fatigue tests performed on the carbon/epoxy composites after sea water aging are shown in Figure 47.a and Figure 47.b for the [0/±45] and [0/90] sequences, respectively.

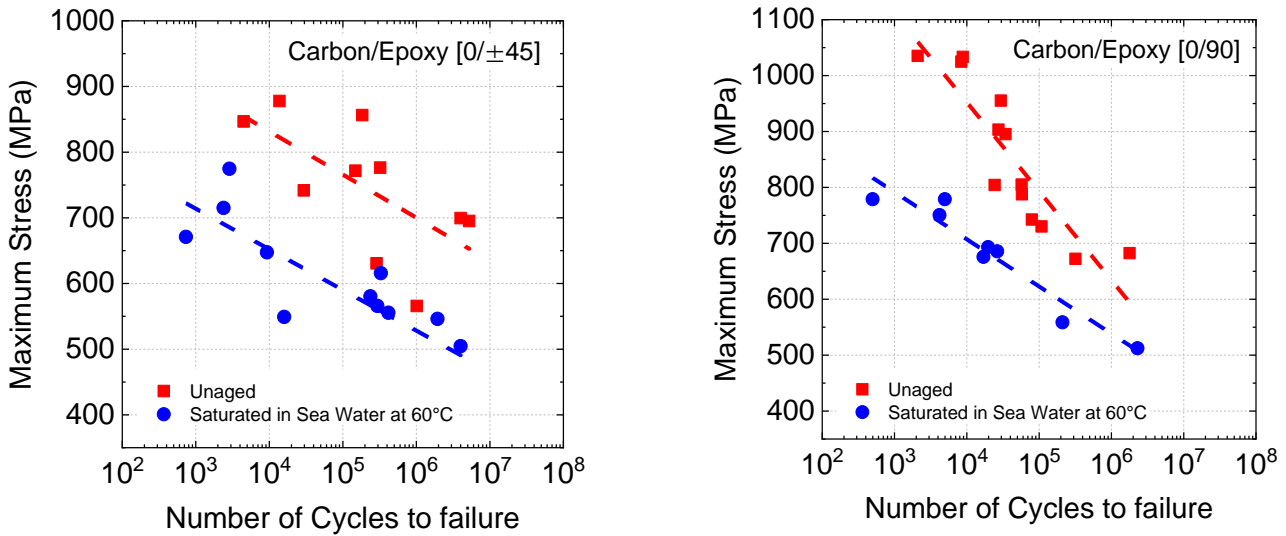


Figure 47: Flexural fatigue tests after sea water aging on carbon/epoxy (a) [0/±45] (b) [0/90]

Results from these two figures show that there is a decrease in the fatigue properties after sea water aging for both materials. While the decrease in fatigue properties observed on the [0/±45] is mostly a shift in the S-N curve, the decrease seen on the [0/90] sequence shows a change in slope. Overall, for both sequences, the decrease in fatigue properties is about 20%.

Results from glass/epoxy composites after sea water aging are shown in Figure 48. It was shown in section 5.2.2 that the static flexural strength decreased by almost 50% after sea water aging, which will surely have an effect on the fatigue curve.

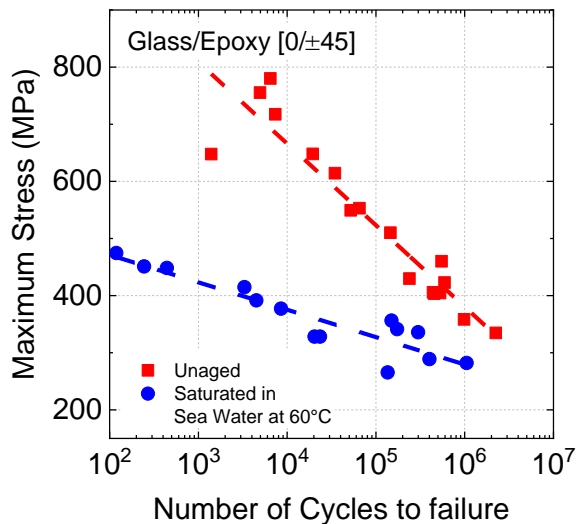


Figure 48: Flexural fatigue tests after sea water aging on glass/epoxy - [0/±45] sequence

Here, results from Figure 48 show that as expected, there is a clear decrease in fatigue properties after sea water aging, more especially at high loads.

Finally, the flexural fatigue results concerning the [0/±45] carbon and glass/epoxy composites before and after aging are shown in Figure 49.

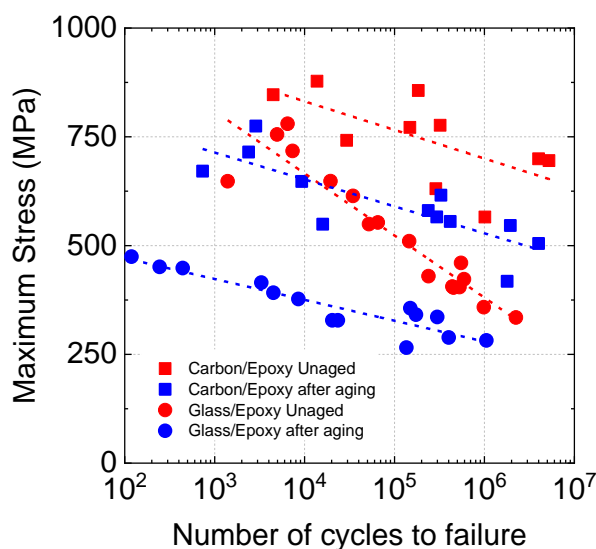


Figure 49: Flexural fatigue tests after sea water aging on carbon and glass/epoxy composites for the [0/±45] stacking sequence

The following conclusion was highlighted many times in this document: the carbon/epoxy composites studied here appear to be better suited for tidal applications than the same matrix reinforced by glass fibres. It is known from published work that glass is usually less suitable for applications subjected to fatigue loadings, however, the gap observed here between the mechanical properties after aging is much greater for glass than for carbon, which was not expected.

### 6.3 Fatigue properties after water desorption

Finally, results from flexural fatigue tests performed on the carbon/epoxy composites with the [0/±45] stacking sequence are shown in Figure 50.

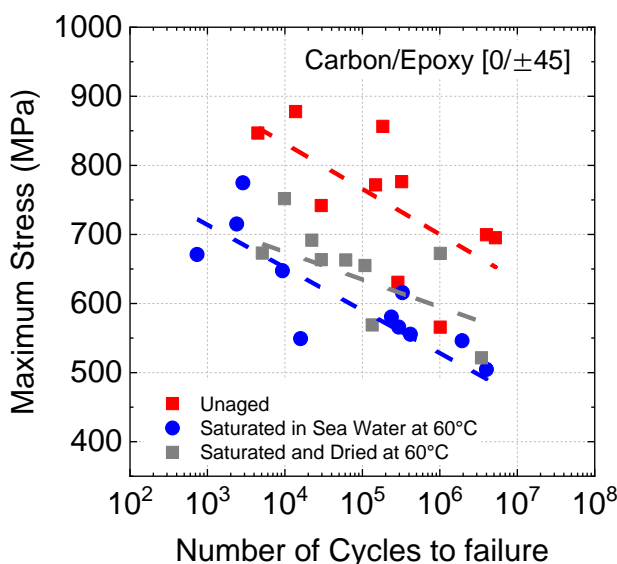


Figure 50: Flexural fatigue tests after desorption on carbon/epoxy

Results from Figure 50 show that the unaged mechanical properties after the desorption process are only partially recovered. This is in agreement with results discussed in section 5.3 on the static properties after desorption. Again, a degradation of the interface upon aging is suggested.

## 7. CONCLUSION

This report presents results from a large test programme in which the influence of seawater aging on the static and cyclic behaviour of composites has been investigated. Unreinforced resin, and composites produced by infusion with the same resin reinforced by glass and carbon fibres, have been studied. The following conclusions can be made:

- Water diffusion models have been proposed to account for water ingress in both resin and composites.
- Accelerated testing using an Arrhenius model can be applied up to a temperature of 60°C. This provides a diffusion acceleration factor compared to 15°C water of 5.25.
- The infused carbon fibre epoxy showed good quality impregnation and excellent mechanical properties before aging. After aging fibre dominated properties were insensitive to aging but for 90° loading a loss of strength was noted.
- Glass fibre composites showed higher manufacturing defect levels and a significant influence of aging on all properties.
- A set of static design data before and after aging is provided.
- Flexural fatigue loading response of both composites is affected by seawater immersion and this must be taken into account in material selection and design.
- Carbon/epoxy composites show longer fatigue lifetimes than glass/epoxy, both before and after saturation in seawater.